J. Fluid Mech. (1999), *vol.* 396, *pp.* 109–141. Printed in the United Kingdom

Numerical studies of transonic BZT gas flows around thin airfoils

By CHUN-WEI WANG† AND ZVI RUSAK

Department of Mechanical Engineering, Aeronautical Engineering and Mechanics, Rensselaer Polytechnic Institute, Troy, NY 12180-3590, USA

(Received 4 June 1998 and in revised form 10 March 1999)

Numerical studies of two-dimensional, transonic flows of dense gases of retrograde type, known as BZT gases, around thin airfoils are presented. The computations are guided by a recent asymptotic theory of Rusak & Wang (1997). It provides a uniformly valid solution of the flow around the entire airfoil surface which is composed of outer and inner solutions. A new transonic small-disturbance (TSD) equation solver is developed to compute the nonlinear BZT gas flow in the outer region around most of the airfoil. The flow in the inner region near the nose of the airfoil is computed by solving the problem of a sonic flow around a parabola. Numerical results of the composite solutions calculated from the asymptotic formula are compared with the solutions of the Euler equations. The comparison demonstrates that, in the leading order, the TSD solutions of BZT gas flows represent the essence of the flow character around the airfoil as computed from the Euler equations. Furthermore, guided by the asymptotic formula, the computational results demonstrate the similarity rules for transonic flows of BZT gases. There are differences between the self-similar cases that may be related to the error associated with the accuracy of the asymptotic solution. A discussion on the flow patterns around an airfoil at transonic speeds and at various upstream thermodynamic conditions is also presented. The paper provides important guidelines for future studies on this subject.

1. Introduction

Dense gases are described as ordinary single-phase vapours with moderate molecular weight operating at pressures, densities, and temperatures around their corresponding thermodynamic critical values (p_c, ρ_c, T_c). For example, gases such as fluorocarbons ($C_nF_{2n+3}N$ or C_nF_{2n-4}, with n normally greater than 10) or hydrocarbons (C_nH_{2n+2}, with n normally greater than 7) have large densities and complex molecular structures along with a large number of degrees of freedom of motion. Therefore, these gases have large heat capacities which may provide a significant heat-to-mechanical energy exchange in closed-cycle power generation systems. In addition to their inert character, the above properties make these gases excellent heat transfer fluids in Rankine cycle turbomachinery (see Devotta & Holland 1985).

The flow of a dense gas ahead of the turbine stage of a power generation system may reach high pressures and temperatures with near sonic speeds. Under these conditions, the perfect gas law cannot adequately predict the thermodynamic and dynamic properties of the gas and real gas effects should be considered. Improved

† Present address: Department of System Engineering, Chung–Cheng Institute of Technology, Ta–Shi, Taoyuan 33509, Taiwan, R.O.C.

equations of state such as the van der Waals (Moran & Shapiro 1992), the Redlich–Kwong (1949), or the Martin–Hou (1955) models should be used for a more accurate description of dense gas flows.

Among those working dense fluids, specific interest has developed in the dense gases of retrograde type. In a certain range of pressures and temperatures, they vaporize when being compressed and condense when being expanded. We particularly investigate the gases that are characterized by relatively large specific heats (c_v), known as the Bethe–Zel'dovich–Thompson (BZT) fluids (see Bethe 1942; Zel'dovich 1946; Zel'dovich & Raizer 1966; Thompson 1971; Thompson & Lambrakis 1973; and Cramer & Tarkenton 1992). Recent research has shown that the physical behaviour of dense gases of retrograde type can be significantly different from the classical gas dynamics of perfect gases (see Cramer & Tarkenton 1992; Cramer & Fry 1993; Kluwick 1993; and Schnerr & Leidner 1993). Therefore, the ability to understand the complex phenomena that occur in compressible flows of dense gases and the parameters that govern them are scientifically interesting and would be essential for future utilization of these fluids in the design of advanced machinery and in aerospace applications.

One of the main parameters commonly used to describe the influence of dense gas effects is the thermodynamic property:

$$\Gamma = 1 + \frac{\rho}{a}\left(\frac{\partial a}{\partial \rho}\right)_s.$$

Here ρ, a, and s are the density, speed of sound, and specific entropy, respectively. A similar parameter was first introduced by Duhem (1909). Due to its importance in a wide range of flow problems, Thompson (1971) referred to this parameter as the fundamental derivative of gasdynamics. This parameter may reflect the intrinsic gasdynamics nonlinearity. For a perfect gas model, $\Gamma = (\gamma + 1)/2$ is a constant and greater than 1 (γ is the ratio of specific heats, $\gamma \geqslant 1$). For dense gases, Γ is no longer a constant and may become less than 1 or even negative in a certain range of temperatures and pressures (see Bethe 1942; Zel'dovich 1946; and Thompson 1971). Fluids, in the single-phase regime, of retrograde type (the BZT fluids) are characterized by $\Gamma < 0$ in some range of densities and pressures (see figures 1 and 2 in Cramer & Tarkenton 1992). A list of commonly used dense fluids which are employed as heat transfer fluids in energy systems or in Rankine cycle power systems, such as the above mentioned high molecular weight hydrocarbons and fluorocarbons, is given in Cramer (1989, 1991), Cramer & Tarkenton (1992), and Tarkenton & Cramer (1993). An example of contours of constant Γ in a pressure–specific volume (p–v) phase diagram, computed according to the van der Waals equation of state with $R/c_v = 0.02$, is shown in figure 1(a) (the Appendix provides the details of the calculations of Γ). The range of pressures and densities where $\Gamma < 0$ is evident in this figure.

In addition to Γ, there are two more nonlinear thermodynamic parameters of interest, the second- and third-nonlinearity parameters:

$$\Lambda = \rho\left(\frac{\partial \Gamma}{\partial \rho}\right)_s, \qquad \Sigma = \rho\left(\frac{\partial \Lambda}{\partial \rho}\right)_s.$$

Examples of contours of constant Λ and Σ in a p–v diagram, computed according to the van der Waals equation of state with $R/c_v = 0.02$, are shown in figures 1(b) and 1(c) (the Appendix provides the details of the calculations of these parameters). It can be seen from figure 1 that, in the range of pressures and densities where turbines

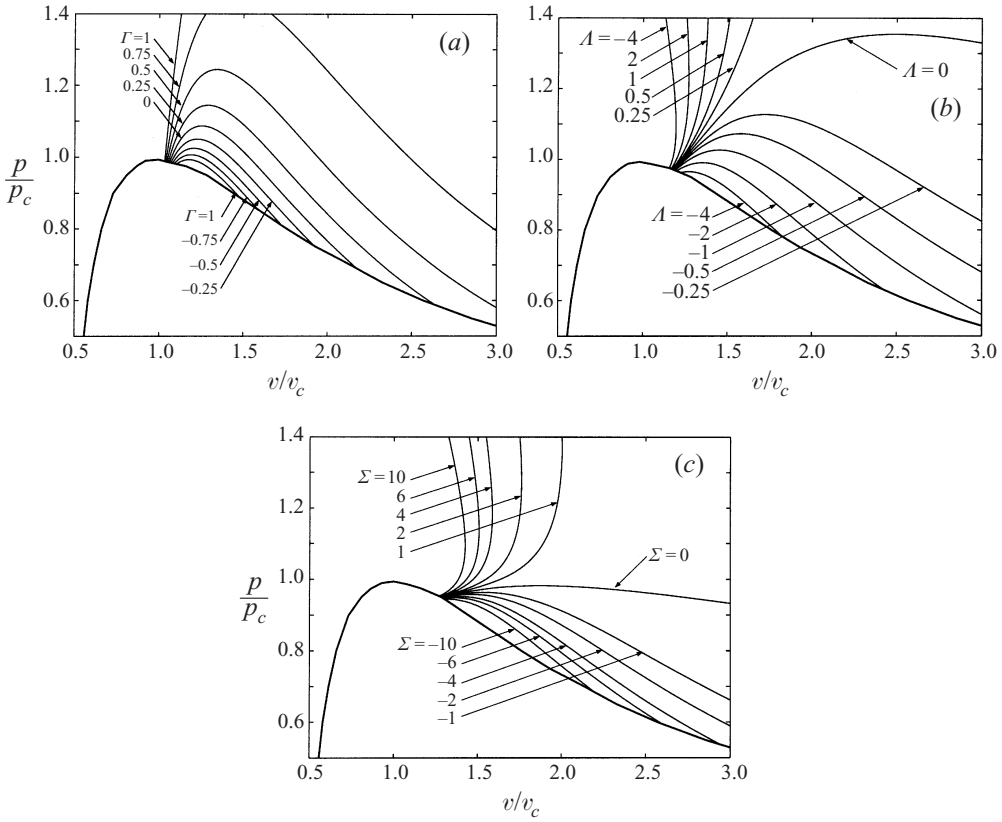

FIGURE 1. (*a*) Constant Γ, (*b*) constant Λ, and (*c*) constant Σ contours using the van der Waals equation of state with $R/c_v = 0.02$.

in a Rankine cycle usually operate, the parameters Γ, Λ, and Σ may change from positive to negative values. Figure 1 is used in the present numerical studies.

Transonic flows of BZT fluids around airfoils have recently been studied by Cramer & Tarkenton (1992) and Tarkenton & Cramer (1993). They presented an extended transonic small-disturbance theory for flows around thin airfoils of thickness ratio $0 < \epsilon \ll 1$. The oncoming flow is near sonic, with Mach number $M_\infty \sim 1$, and is also characterized by small values of Γ, $\Gamma_\infty \sim 0$, as well as the second-nonlinearity parameter Λ, $\Lambda_\infty \sim 0$. The third-nonlinearity parameter, Σ, is considered to be of order one, $\Sigma_\infty \sim O(1)$. The basic shape functions of the upper and lower surfaces of the airfoil, $F_{u,l}(x)$, as well as several similarity parameters relating M_∞, Γ_∞, Λ_∞ and ϵ were fixed. Using this special theory, Tarkenton & Cramer (1993) found a significant increase of the critical Mach number in flows of the BZT fluids over airfoils. Numerical solutions revealed substantial reductions in the strength of compression shocks waves. A further benefit is an evident decrease of the pressure drag that was found in the numerical study of Morren (1990) using the Euler equations and the van der Waals equation of state. Although the van der Waals equation of state is known to overestimate non-classical effects, it seems to be well suited to numerical simulation of qualitative effects of dense gas flows.

Morren's (1990) code is a modified version of Jameson & Yoon's (1986) finite volume code and it uses the flux splitting technique to capture shock waves. Her

computations also revealed the special, non-classical behaviour of the BZT gases which is the formation of expansion shock waves on the airfoil, where $\Gamma < 0$ ahead of the shock wave. This interesting phenomenon indicates that the increase in the speed of sound across the expansion shock wave is more than the increase in the speed of the flow to maintain the Mach number behind the shock wave below 1. The computations also show the appearance of a detached shock wave in front of the airfoil although the Mach number in the far field is less than 1. This special behaviour of the flow is, again, contrary to the perfect gas behaviour.

Transonic flow of a dense gas of retrograde type around the leading edge of a thin airfoil with a parabolic nose has been studied by Rusak & Wang (1997). Asymptotic expansions of the velocity potential function were constructed in terms of the airfoil thickness ratio in an outer region around the airfoil and in an inner region near the nose. The outer expansion consisted of the transonic small-disturbance theory for the BZT gases, where a leading-edge singularity appears. Analytical expressions were given for this singularity by constructing similarity solutions of the governing nonlinear equation. The inner expansion accounted for the flow around the nose, where a stagnation point exists. A boundary value problem was formulated in the inner region. It involves the solution of an oncoming uniform sonic flow with zero values of the fundamental derivative of gasdynamics ($\Gamma = 0$) and the second-nonlinearity parameter ($\Lambda = 0$) around a semi-infinite parabola at zero angle of attack. The numerical solution of the inner problem resulted in a symmetric flow around the nose. The outer and inner expansions were matched asymptotically, resulting in a uniformly valid solution along the entire airfoil surface. In the leading terms, the flow around the nose is symmetric and the stagnation point is located at the leading edge for every transonic Mach number, small values of Γ and Λ of the oncoming flow, and any shape and small angle of attack of the airfoil. Furthermore, analysis of the inner region in the immediate neighbourhood of the stagnation point revealed that the flow there is purely subsonic and approaches critical conditions in the limit of large (scaled) distances. This excludes the formation of shock discontinuities in the nose region. It should be clarified that the theory of Rusak & Wang (1997) holds only for the cases where M_∞ is near 1 and Γ_∞, Λ_∞ are near zero.

In the present paper we demonstrate the agreement between the special asymptotic theory of Rusak & Wang (1997) and the numerical solutions of the Euler equations of Morren (1990). The outline of the paper is as follows: the asymptotic theory of Rusak & Wang (1997) is reviewed and the details needed to construct the uniformly valid solution for the flow around the entire airfoil surface are provided (§ 2). A new transonic small-disturbance (TSD) equation solver is developed to compute the non-linear BZT gas flow in the outer region around most of the airfoil (§ 3). Numerical results of the composite solutions calculated from the asymptotic formula are compared with the solutions of the Euler equations (§ 4). The comparison demonstrates that, in the leading order, the TSD solutions of the BZT gas flows represent the essence of the flow character computed from the Euler equations. Furthermore, guided by the asymptotic formula, the computational results demonstrate the similarity rules for transonic flow of BZT gases. The differences between the self-similar cases are discussed. A discussion on the flow patterns around an airfoil at transonic speeds and at various upstream thermodynamic conditions is also presented. It provides important guidelines for future studies on this subject.

The TSD theory provides a special insight into the behaviour of solutions of the Euler equations. The theory results in a simplified form of the Euler equations from which the basic similarity relations between the various flow and thermodynamic

parameters may be revealed. Such relations cannot be found from numerical simulations using the Euler equations. These parameters help to guide the numerical studies using both the small-disturbance theory and the Euler equations (see §4). Moreover, the agreement found in this paper between the results from the two methods, which are essentially independent of each other, provides a unique check on both methods, although there are some important differences that are discussed in the paper (see §4). One more advantage of using the TSD theory over the Euler computations is the fact that no specific equation of state has to be coupled with the main equation in studying the flow behaviour. The similarity parameters in the equation can be computed by using any equation of state.

As mentioned above, the asymptotic theory holds for the limited range of upstream thermodynamic conditions where Γ_∞ and Λ_∞ are around zero. However, in this range of parameters the BZT gases change their nature from a classical behaviour to a non-classical, retrograde gas behaviour. Significant changes in the flow pattern and aerodynamic performance can be found by slightly changing the values of these parameters in the above range (see §4.4). The TSD theory helps to unfold these significant changes.

The results of this study may add to our understanding of the complicated physics of compressible flows of dense gases. We expect that the BZT gases offer numerous advantages in turbomachinery applications, because they have the potential of supporting subsonic flow at a higher free-stream Mach number and/or blade angle of attack without encountering any shock waves. This may also help to reduce boundary layer flow separation caused by strong shock waves.

2. Mathematical model

2.1. *Assumptions and basic equations*

A steady, attached, compressible two-dimensional flow of dense gas around a thin airfoil with a parabolic nose at a low angle of attack is considered in an (x, y)-plane with unit vectors $\boldsymbol{e}_x$ and $\boldsymbol{e}_y$. The airfoil's shape is described by the equation $B(x, y) = 0$ where $0 \leqslant x \leqslant c$ and c is the airfoil's chord. The flow far ahead of the airfoil is uniform and is characterized by speed U_∞ in the x-direction, that is near the speed of sound, and pressure, p_∞, and density, ρ_∞, on the order of the critical pressure and density of the gas.

Since in high Reynolds number attached flows the boundary layer thickness is relatively small compared to the airfoil thickness, the viscous effects may be neglected and the flow can be considered as inviscid. The flow may be described by the two-dimensional and steady Euler equations,

$$\left.\begin{aligned} \text{continuity:}\quad & \nabla\cdot(\rho\boldsymbol{U}) = 0, \\ \text{momentum:}\quad & \rho\boldsymbol{U}\cdot\nabla\boldsymbol{U} = -\nabla p, \\ \text{energy:}\quad & h + \tfrac{1}{2}U^2 = \text{constant}, \end{aligned}\right\} \tag{1}$$

and the entropy condition according to the second law of thermodynamics. Here h is the flow local specific enthalpy, $\boldsymbol{U}$ is the local velocity vector, and $U^2 = \boldsymbol{U}\cdot\boldsymbol{U}$. The equation of state relating the thermodynamic properties should also be specified, $h = h(\rho, s)$. This relation may be described by the van der Waals equation of state or any other relevant model such as the Redlich–Kwong or the Martin–Hou equations.

The flow has to satisfy the tangency (no penetration) condition at any point along the airfoil surfaces, $\boldsymbol{U}\cdot\nabla B = 0$ for every x and y on $B(x, y) = 0$. Far away from

the airfoil, the flow has to decay to uniform flow conditions, specifically ahead of the airfoil, i.e. $\boldsymbol{U} \to U_\infty \boldsymbol{e}_x$, $p \to p_\infty$ and $\rho \to \rho_\infty$. The Kutta condition describing the continuity of pressure and the tangency of the upper and lower streams at a sharp trailing edge should be satisfied. Also, in order to have a single-valued solution, the (x, y)-plane is cut along the slipstream that leaves the airfoil's trailing edge to infinity.

From the momentum and energy equations (1) and the Gibbs relation (Moran & Shapiro 1992)

$$\mathrm{d}h = T\,\mathrm{d}s + v\,\mathrm{d}p, \tag{2}$$

where s is the local specific entropy and $v = 1/\rho$ is the specific volume, it can be shown that

$$T\nabla s = -\boldsymbol{U} \times \Omega. \tag{3}$$

This is Crocco's theorem for any gas. Here $\Omega = \nabla \times \boldsymbol{U}$ is the vorticity vector. Multiplying (3) by $\boldsymbol{U}$ gives $\boldsymbol{U} \cdot \nabla s = 0$. This means that in continuous flow regions the specific entropy is constant along a stream line, but it changes from one value to another across a shock wave. Since the upstream flow is uniform and all stream lines originate from there, we have $s = s_\infty$ along stream lines ahead of a shock wave and $s = s_\infty + \Delta s$ behind a shock wave. According to the second law of thermodynamics, the change in entropy, Δs, must be positive.

Transonic flows are usually characterized by the appearance of relatively weak shock waves. An estimation of the entropy jump across a weak shock wave (Thompson 1984 or Wang 1998) shows that

$$\frac{T[s]}{a^2} = \frac{\Gamma}{6a^6\rho^3}[p]^3 + \cdots . \tag{4}$$

For a perfect gas, it can be shown that $\Gamma = (\gamma + 1)/2 =$ constant in the entire flow field, where γ is the ratio of specific heats, $\gamma = c_p/c_v$, of the working fluid. Thus, the specific entropy jump across a shock wave in a perfect gas is on the order of $[p]^3$. However, for some dense gases, such as the BZT gases, there may exist a range of pressures and densities where Γ and Λ have small values around zero (either positive or negative). When Γ is on the order of $[p]^2$ and Λ is on the order of $[p]$, it is found that the specific entropy jump $[s]$ across shock waves in these dense gases is on the order of $[p]^5$ (see Thompson 1984). A steady, inviscid dense gas flow at transonic speeds with small disturbances in the speed, pressure, density, and enthalpy is characterized by much smaller changes of the specific entropy and the flow may be considered, in the leading orders of the disturbances, as isentropic.

It should also be emphasized that, from Crocco's relation, the change of entropy is related to the change of vorticity. Since the change of entropy across a weak shock in a BZT gas is on the order of $[p]^5$, it is concluded that the change of vorticity is also on the same order, i.e. to the leading order of disturbances the flow may also be considered as irrotational.

2.2. *Asymptotic theory*

A thin airfoil with a parabolic nose is considered, where

$$B(x, y) = y - \epsilon c F_{u,l}(x/c) = 0 \quad \text{for} \quad 0 \leqslant x \leqslant c. \tag{5}$$

Here c is the airfoil's chord and ϵ is the thickness ratio, $\epsilon \ll 1$. The functions $F_{u,l}(x/c)$ represent the upper and lower surfaces, respectively. These shape functions are given by

$$F_{u,l}(x) = Ca(x/c) \pm t(x/c) - \Theta x/c \quad \text{for} \quad 0 \leqslant x \leqslant c, \tag{6}$$

where $Ca(x/c)$ is the camber line function, $t(x/c)$ is the thickness distribution, $\Theta = \theta/\epsilon$, and θ is the angle of attack. Also, $t(0) = t(1) = 0$ and $Ca(0) = Ca(1) = 0$. Near the airfoil's leading edge, $y = \pm 2g\epsilon\sqrt{cx} + \cdots$ where g is a constant related to the radius of curvature of the parabolic nose.

The flow far ahead of the airfoil is assumed to be uniform at a speed U_∞, density ρ_∞, entropy s_∞, speed of sound a_∞, and Mach number $M_\infty \equiv U_\infty/a_\infty \sim 1$. The oncoming flow is also characterized by small values of the fundamental derivative of gasdynamics ($\Gamma_\infty \sim 0$) and the second-nonlinearity parameter ($\Lambda_\infty \sim 0$), and the third-nonlinearity parameter of order 1 ($\Sigma_\infty \sim O(1)$). As shown in the previous subsection, to the orders of the disturbances in the pressure, density, and velocity vector considered here, the flow may be taken as irrotational and isentropic, i.e. $s \sim s_\infty$ and $\Omega \sim 0$ everywhere in the flow domain. The velocity potential field $\Phi(x, y)$ of the flow, where $\boldsymbol{U} = \nabla\Phi$ (Φ_x is the axial speed and Φ_y is the vertical speed), can be described by the full potential-flow equation:

$$(a^2 - \Phi_x^2)\Phi_{xx} - 2\Phi_x\Phi_y\Phi_{xy} + (a^2 - \Phi_y^2)\Phi_{yy} = 0 \tag{7}$$

and the energy equation:

$$h(\rho, s_\infty) + \tfrac{1}{2}\,|\nabla\Phi|^2 = h_\infty + \tfrac{1}{2}U_\infty^2. \tag{8}$$

Here, $h_\infty = h(\rho_\infty, s_\infty)$. Also, $a = a(\rho, s_\infty)$ and $p = p(\rho, s_\infty)$. The energy equation relates the disturbances in the speed of sound to those in Φ through the thermodynamic relations between a and h. The solution of (7) and (8) should satisfy the kinematic tangency boundary condition on the airfoil surface:

$$\nabla\Phi \cdot \nabla B = 0 \quad \text{on} \quad B = 0. \tag{9}$$

Also, disturbances must die out at upstream infinity, as $x \to -\infty$: $\Phi_x \to U_\infty$ and $\Phi_y \to 0$. The potential Φ is allowed to jump along the cut from the airfoil's trailing edge to infinity due to the circulation around the airfoil.

Rusak & Wang (1997) have recently shown that the potential Φ can be approximated by asymptotic expansions in an outer region, around most of the airfoil, where the flow perturbations are small, and a small inner region, on the order of ϵ^2, around the nose of the airfoil where the flow approaches stagnation and the flow perturbations are large. The matching between the two expansions results in a uniformly valid approximate solution for the flow field around the entire airfoil:

$$\Phi(x, y; \epsilon, M_\infty, \Theta, \Gamma_\infty, \Lambda_\infty, \Sigma_\infty) \sim U_\infty c\big\{\bar{x} + \epsilon^{2/5}\bar{\phi}(\bar{x}, \tilde{y}; K, K_\Gamma, K_\Lambda, \Sigma_\infty) + \epsilon^2\left(x^* + \phi_0(x^*, y^*)\right) - \Phi_{c.p.}\big\}. \tag{10}$$

Here $\bar{\phi}$ is the small-disturbance potential in the outer region and is determined by the transonic small-disturbance (TSD) theory for the BZT gases,

$$\left(-K + 2K_\Gamma\,\bar{\phi}_{\bar{x}} - K_\Lambda\bar{\phi}_{\bar{x}}^2 + \tfrac{1}{3}\Sigma_\infty\bar{\phi}_{\bar{x}}^3\right)\bar{\phi}_{\bar{x}\bar{x}} = \bar{\phi}_{\tilde{y}\tilde{y}}, \tag{11}$$

where

$$\bar{x} = \frac{x}{c},\ \bar{y} = \frac{y}{c},\ \tilde{y} = \epsilon^{3/5}\bar{y},\ M_\infty^2 = 1 - \epsilon^{6/5}K,\ \Gamma_\infty = \epsilon^{4/5}K_\Gamma,\ \Lambda_\infty = \epsilon^{2/5}K_\Lambda. \tag{12}$$

This equation is a modified Kármán–Guderley (K–G) equation (see also Kluwick 1993 and Tarkenton & Cramer 1993). The function $\bar{\phi}_1$ should satisfy the following

boundary and upstream conditions:

$$\left.\begin{aligned} &\bar{\phi}_{\bar{y}}(\bar{x},0\pm) = F'_{u,l}(\bar{x}) \quad \text{for} \quad 0 \leqslant \bar{x} \leqslant 1, \\ &\bar{\phi}_{\bar{x}}, \bar{\phi}_{\bar{y}} \to 0 \quad \text{as} \quad \bar{x} \to -\infty, \\ &\bar{\phi}_{\bar{x}}(1,0^+) = \bar{\phi}_{\bar{x}}(1,0^-). \end{aligned}\right\} \tag{13}$$

In order to formulate a one-valued potential function $\bar{\phi}$, we have $\bar{\phi}(\bar{x},0^+) - \bar{\phi}(\bar{x},0^-) = C$ for every $\bar{x} \geqslant 1$, where C is the circulation around the airfoil. Note from (10) that the pressure perturbation is $O(\epsilon^{2/5})$. From (4) and (12) we find that the entropy change across any shock wave in the flow is $O(\epsilon^2)$ and is indeed much smaller than the changes in the velocity and pressure as assumed above.

Also in (10), $x^* = \bar{x}/\epsilon^2, y^* = \bar{y}/\epsilon^2$ are the inner region variables, and $\phi_0(x^*, y^*)$ is a solution of

$$\left(\frac{a^2}{U_\infty^2} - (1+\phi_{0x^*})^2\right)\phi_{0x^*x^*} - 2(1+\phi_{0x^*})\phi_{0y^*}\phi_{0x^*y^*} + \left(\frac{a^2}{U_\infty^2} - \phi_{0y^*}^2\right)\phi_{0y^*y^*} = 0 \tag{14}$$

with the energy equation

$$h^*(\rho, s_\infty) + \tfrac{1}{2}U_\infty^2\left((1+\phi_{0x^*})^2 + \phi_{0y^*}^2\right) = h_\infty + \tfrac{1}{2}U_\infty^2. \tag{15}$$

Here, h^* is the specific enthalpy in the inner region problem and the speed of sound $a(x^*, y^*)$ is calculated from the thermodynamic relation between a and h^*. The boundary condition over the airfoil surface becomes, in the inner region,

$$\phi_{0y^*}\left(x^*, y^* = \pm 2g\sqrt{x^*}\right) \mp \frac{g}{\sqrt{x^*}}\left(1 + \phi_{0x^*}\left(x^*, y^* = \pm 2g\sqrt{x^*}\right)\right) = 0. \tag{16}$$

The upstream condition for the inner problem is $(\phi_{0x^*}, \phi_{0y^*}) \to 0$ as $x^* \to -\infty$. The problem given by (14)–(16) describes, in the (x^*, y^*)-plane, a sonic uniform flow with speed $a_\infty \boldsymbol{e}_{x^*}$ and $\Gamma_\infty = \Lambda_\infty = 0$ around a semi-infinite parabola surface: $y^* = \pm 2g\sqrt{x^*}$.

The common part of the potential,

$$\Phi_{c.p.} = \eta x_\eta + \phi_{c.p.}, \tag{17}$$

is derived from the matching between the outer and inner expansions in an intermediate region. This region, $\eta(\epsilon)$, is chosen such that $\epsilon^2 \ll \eta(\epsilon) \ll 1$, and there, $x_\eta = \bar{x}/\eta(\epsilon)$, $y_\eta = \bar{y}/\eta(\epsilon)$ are fixed in the limit $\epsilon \to 0, M_\infty \to 1, \Gamma_\infty \to 0, \Lambda_\infty \to 0$. Also,

$$\phi_{c.p.} = \epsilon^{2/5} E^{-1/3} \tilde{y}^{8/13} f(\xi), \tag{18}$$

where $E = \Sigma_\infty/3$, $\xi = \bar{x}/\tilde{y}^{10/13}$ and $f(\xi)$ is given by the parametric representation:

$$\xi(\alpha) = -\tfrac{1}{2}\left(\tfrac{5}{2}\right)^{3/5} c_1^{3/13} \frac{\cos^{8/5}\alpha \; F(\frac{9}{5}, -\frac{1}{2}; \frac{1}{2}; \sin^2\alpha)}{\sin^{10/13}\alpha \; F^{10/13}(\frac{9}{5}, -\frac{1}{2}; \frac{3}{2}; \sin^2\alpha)}, \tag{19}$$

$$f(\alpha) = c_1^{5/13} \frac{26\sin^2\alpha F(\frac{9}{5}, -\frac{1}{2}; \frac{3}{2}; \sin^2\alpha) + 25\cos^2\alpha \; F(\frac{9}{5}, -\frac{1}{2}; \frac{1}{2}; \sin^2\alpha)}{16[\sin\alpha \; F(\frac{9}{5}, -\frac{1}{2}; \frac{3}{2}; \sin^2\alpha)]^{8/13}}. \tag{20}$$

Here $c_1 = 1.768163g^2$, $-75.383226^\circ \leqslant \alpha \leqslant 75.383226^\circ$, and $F(a, b; c; z)$ is the standard hypergeometric function (Abramowitz & Stegun 1965).

From the composite solution (10), the relation (17), and the energy equation in (1),

the specific enthalpy in the flow field may be approximated by

$$\begin{aligned} h &= h_\infty + \frac{U_\infty^2}{2}\left(1 - \frac{\Phi_x^2 + \Phi_y^2}{U_\infty^2}\right) \\ &= h_\infty + \tfrac{1}{2}M_\infty^2 a_\infty^2\left(1 - (1+\phi_{0x^*})^2 - \phi_{0y^*}^2 - 2\epsilon^{2/5}(1+\phi_{0x^*})\left(\bar{\phi}_{1\bar{x}} - \bar{\phi}_{c.p.\bar{x}}\right) + \cdots\right) \\ &= h^*(x^*, y^*) - \epsilon^{2/5} M_\infty^2 a_\infty^2 (1+\phi_{0x^*})\left(\bar{\phi}_{1\bar{x}} - \bar{\phi}_{c.p.\bar{x}}\right) \\ &\quad -\tfrac{1}{2}\left(1 - M_\infty^2\right) a_\infty^2\left(1 - (1+\phi_{0x^*})^2 - \phi_{0y^*}^2\right) + \cdots . \end{aligned} \tag{21}$$

From (21), we find

$$\begin{aligned} c_h = \frac{h - h_\infty}{a_\infty^2} &= \frac{h^*(x^*, y^*) - h_\infty}{a_\infty^2} \\ &\quad + \left(1 + \phi_{0x^*}(x^*, y^*)\right)\frac{h_{TSD} - h_{c.p.}}{a_\infty^2} + O(\epsilon^{4/5}, |1 - M_\infty^2|). \end{aligned} \tag{22}$$

Here $h^*(x^*, y^*)$ and $1 + \phi_{0x^*}(x^*, y^*)$ are the specific enthalpy and axial velocity component in the inner flow problem, respectively. Also, $(h_{TSD} - h_\infty)/a_\infty^2 = -\epsilon^{2/5}\bar{\phi}_{1\bar{x}}$ is the specific enthalpy change in the outer (TSD) flow problem and $(h_{c.p.} - h_\infty)/a_\infty^2 = -\epsilon^{2/5}E^{-1/3}\tilde{y}^{-2/13}f_{\tilde{\xi}}$ is the specific enthalpy change of the common part in the overlap region.

Since the pressure is given by $p = p(h, s_\infty)$ we can use (21) to derive an asymptotic expansion for p:

$$\begin{aligned} p &= p(h^*) - \left(\frac{\partial p}{\partial h}\right)_s^* \epsilon^{2/5} M_\infty^2 a_\infty^2 (1+\phi_{0x^*})\left(\bar{\phi}_{1\bar{x}} - \bar{\phi}_{c.p.\bar{x}}\right) + \cdots \\ &= p^*(x^*, y^*) + \rho^*(x^*, y^*)\epsilon^{2/5} M_\infty^2 a_\infty^2 (1+\phi_{0x^*})\left(\bar{\phi}_{1\bar{x}} - \bar{\phi}_{c.p.\bar{x}}\right) + \cdots . \end{aligned} \tag{23}$$

We use here the relation $(\partial p/\partial h)_s^* = \rho^*$, which results from the Gibbs equation (2). From the definition of the pressure coefficient, c_p, we have

$$\begin{aligned} c_p = \frac{p - p_\infty}{\frac{1}{2}\rho_\infty U_\infty^2} &= \frac{p/p_\infty - 1}{\frac{1}{2}BM_\infty^2} \\ &= c_p^* + \frac{\rho^*}{\rho_\infty}(1+\phi_{0x^*})\left(c_{pTSD} - c_{p_{c.p.}}\right) + O(\epsilon^{4/5}, |1 - M_\infty^2|). \end{aligned} \tag{24}$$

Here c_p^*, ρ^*, and $(1 + \phi_{0x^*})$ are the pressure coefficient, density, and axial velocity component in the inner flow problem, respectively. Also, $c_{pTSD} = -2\epsilon^{2/5}\bar{\phi}_{1\bar{x}}$ is the pressure coefficient in the outer (TSD) flow problem and $c_{p_{c.p.}} = -2\epsilon^{2/5}E^{-1/3}\tilde{y}^{-2/13}f_{\tilde{\xi}}$ is the common part of the pressure coefficient in the overlap region. Also, the parameter $B = \rho_\infty a_\infty^2/p_\infty$.

Equations (22) and (24) show that both the specific enthalpy and pressure coefficient at any point are composed of the nose effect and the airfoil small-disturbance influence. As the leading edge of the airfoil is approached, $(x, y) \to 0$ or $0 \leqslant \sqrt{x^2 + y^2} < \epsilon^2 g^2 c$, the common part of the specific enthalpy, $h_{c.p.}$, or the common part of the pressure coefficient, $c_{p_{c.p.}}$, cancel the nose singularity of the outer region. Also, in this region, the axial velocity $1 + \phi_{0x^*}(x^*, y^*)$ is small and tends to zero near the stagnation point. Therefore, the dominant terms in the leading-edge region are the inner-region specific enthalpy, h^*, and pressure coefficient, c_p^*. As (x, y) increase beyond

the leading-edge region, $\sqrt{x^2+y^2} \gg \epsilon^2 g^2 c$, the axial velocity $1+\phi_{0x^*}(x^*,y^*)$ and density $\rho^*(x^*,y^*)/\rho_\infty$ approach 1. Also, the common part of the enthalpy and pressure coefficient tend to cancel the inner-region enthalpy, h^*, and pressure coefficient, c_p^*. Therefore, the dominant terms outside the leading-edge region are the TSD terms h_{TSD} and c_{pTSD}. In the intermediate region, the enthalpy and pressure coefficient change uniformly from h^* to h_{TSD} and c_p^* to c_{pTSD}, respectively.

In § 4, we compare results according to the approximate solutions (22) and (24) with results from numerical simulations using equations (1). The TSD problem provides the similarity parameters (12) that may govern the flow problem and these are used in the present work as guiding parameters for studying the various cases. We find good agreement between the approximate solutions and the results from the numerical simulations. Moreover, flow cases characterized by the same similarity parameters show a qualitative self-similar behaviour. It should be pointed out, however, that the similarity parameters (12) result from an asymptotic solution of the problem and not from the full nonlinear flow behaviour. Therefore, some differences are expected in the comparison between the asymptotic solutions based on the TSD problem and those of (1). Specifically, these differences can be found in the location of shock waves along the airfoil's chord and may be related to the small entropy production behind the shock waves that exists in the solutions of (1) and is neglected in the TSD problem. Shock wave locations of the self-similar cases can differ by up to 10% of the airfoil's chord. A similar difficulty can be seen in comparing solutions of the TSD problem for a perfect gas with solutions of the Euler equations (see, for example, Cole & Cook 1986, pp. 312–320).

It should also be clarified that the asymptotic solution (24) contains an error of $O(\epsilon^{4/5}, |1-M_\infty^2|)$. This error is greater than $O(\epsilon)$. It is also much greater than the error typically found in the asymptotic solutions for the perfect gas flow, which is $O(\epsilon^{4/3}) < O(\epsilon)$ (see Cole & Cook 1986 and Rusak 1993). For example, for airfoils with $\epsilon = 0.12$ the local error of the asymptotic solution may be on the order of 20%. This difference becomes more noticeable when we use the self-similar, scaled (magnified) pressure coefficient $c_p' = c_p/\epsilon^{2/5}$. This parameter may contain an error on the order of $O(\epsilon^{2/5})$ which is much greater than the error typically found in the asymptotic solutions for the perfect gas case, $O(\epsilon^{2/3})$. For example, for airfoils with $\epsilon = 0.12$ the local error in computing the scaled pressure c_p' at points around the maximum thickness of the airfoil may be on the order of 40–50% (unlike the perfect gas case where such an error is typically less than 20%). It is expected that the error becomes smaller as ϵ is reduced. This error indicates the need to develop a second-order theory for transonic flow of the BZT gases to improve the computational accuracy of the asymptotic formula, specifically for airfoils with $\epsilon > 0.1$.

3. The TSD equation solver

The TSD problem is described by (11)–(13). It can be shown that the local Mach number, M_l, is given by

$$M_l^2 = 1+\epsilon^{6/5}\left(-K+2K_\Gamma \bar{\phi}_{1\bar{x}} - K_\Lambda \bar{\phi}_{1\bar{x}}^2 + \tfrac{1}{3}\Sigma_\infty \bar{\phi}_{1\bar{x}}^3\right) + \cdots = 1+\epsilon^{6/5}\chi + \cdots . \quad (25)$$

From the definition of χ, the modified K–G equation (11) can be written as

$$\chi \bar{\phi}_{1\bar{x}\bar{x}} = \bar{\phi}_{1\bar{y}\bar{y}}. \quad (26)$$

When $\chi > 0$, the local flow is supersonic ($M_l > 1$) and from (26) the modified K–G equation is hyperbolic. On the other hand, when $\chi < 0$, the local flow is subsonic

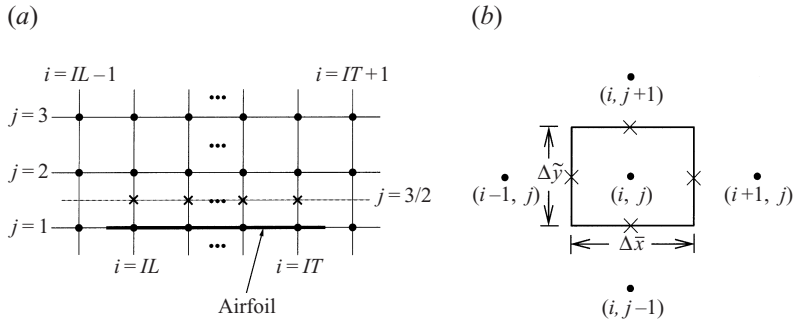

FIGURE 2. (*a*) The computational grid points around the airfoil, and (*b*) a control volume and nearby grid points, in the TSD solver.

($M_l < 1$) and the modified K–G equation is elliptic. When $\chi = 0$, the local flow is sonic ($M_l = 1$) and the equation is parabolic. These criteria play an important role in the numerical scheme for solving the TSD problem for the BZT gases given by (11)–(13). This mixed-type problem requires a type-sensitive difference scheme, such as the Murman & Cole (1971) method (see also Cole & Cook 1986), to catch adequate and relevant solutions of transonic flows of the BZT gases. In every iteration of the computations and at each computational grid point, a test has to be devised to decide whether the governing equation at this point is of elliptic, hyperbolic, or mixed type. Then, an appropriate difference scheme to solve the equation at that point has to be used.

For numerical consistency, a conservative form of (11) is used to contain the shock jump relations, i.e.

$$\left(-K\bar{\phi}_{\bar{x}} + K_\Gamma \bar{\phi}_{\bar{x}}^2 - \tfrac{1}{3}K_\Lambda \bar{\phi}_{\bar{x}}^3 + \tfrac{1}{12}\Sigma_\infty \bar{\phi}_{\bar{x}}^4\right)_{\bar{x}} = \left(\bar{\phi}_{\tilde{y}}\right)_{\tilde{y}}. \tag{27}$$

Note that in the surroundings of the state $\Gamma_\infty = \Lambda_\infty = 0$ (or $K_\Gamma = K_\Lambda = 0$) we find $\Sigma_\infty/12 > 0$. Therefore, the operator $-K\bar{\phi}_{\bar{x}} + K_\Gamma \bar{\phi}_{\bar{x}}^2 - K_\Lambda \bar{\phi}_{\bar{x}}^3/3 + \Sigma_\infty \bar{\phi}_{\bar{x}}^4/12$ is typically convex in terms of $\bar{\phi}_{\bar{x}}$ in this range of upstream conditions. Thus, an extended version of the Murman & Cole (1971) method may be relevant to numerically solve (27).

The flow domain is divided into a uniform finite difference mesh with equal spacing $\Delta\bar{x}$ and $\Delta\tilde{y}$ and with grid points labelled by (i, j). The $j = 1$ line is assigned on the body surface and the boundary condition in (13) is set on the line $j = \frac{3}{2}$ (see figure 2*a*). From the control volume diagram around a grid point (i, j) (figure 2*b*), the finite difference equation at this point is

$$\begin{aligned}&\left\{\left(-K\bar{\phi}_{\bar{x}} + K_\Gamma \bar{\phi}_{\bar{x}}^2 - \tfrac{1}{3}K_\Lambda \bar{\phi}_{\bar{x}}^3 + \tfrac{1}{12}\Sigma_\infty \bar{\phi}_{\bar{x}}^4\right)_{i+1/2,j}\right.\\ &\quad\left.-\left(-K\bar{\phi}_{\bar{x}} + K_\Gamma \bar{\phi}_{\bar{x}}^2 - \tfrac{1}{3}K_\Lambda \bar{\phi}_{\bar{x}}^3 + \tfrac{1}{12}\Sigma_\infty \bar{\phi}_{\bar{x}}^4\right)_{i-1/2,j}\right\}\Delta\tilde{y}\\ &\quad-\left\{\left(\bar{\phi}_{\tilde{y}}\right)_{i,j+1/2} - \left(\bar{\phi}_{\tilde{y}}\right)_{i,j-1/2}\right\}\Delta\bar{x} = 0.\end{aligned} \tag{28}$$

Here the $i \pm \frac{1}{2}$ and $j \pm \frac{1}{2}$ indicate the positions of the boundary of the control volume in terms of the grid numbers in the $\bar{x}$- and $\tilde{y}$-directions, respectively. Several basic types of difference methods are applied to (28). In the $\tilde{y}$-direction, the difference of the velocities between two consecutive grid points is described by a central difference

method:

$$\left(\bar{\phi}_{\bar{y}}\right)_{i,j+1/2} = \frac{\bar{\phi}_{i,j+1} - \bar{\phi}_{i,j}}{\Delta\tilde{y}}\,, \quad \left(\bar{\phi}_{\bar{y}}\right)_{i,j-1/2} = \frac{\bar{\phi}_{i,j} - \bar{\phi}_{i,j-1}}{\Delta\tilde{y}}.$$

In the $\bar{x}$-direction, the flow may become subsonic, sonic, supersonic, or encounter a shock wave. Since the flow may change its speed, the type of the TSD equation may change and, thus, we need to examine the following difference methods:
central difference

$$\left(\bar{\phi}_{\bar{x}}\right)^{(C)}_{i+1/2,j} = \frac{\bar{\phi}_{i+1,j} - \bar{\phi}_{i,j}}{\Delta\bar{x}}\,, \quad \left(\bar{\phi}_{\bar{x}}\right)^{(C)}_{i-1/2,j} = \frac{\bar{\phi}_{i,j} - \bar{\phi}_{i-1,j}}{\Delta\bar{x}},$$

backward difference

$$\left(\bar{\phi}_{\bar{x}}\right)^{(B)}_{i+1/2,j} = \frac{\bar{\phi}_{i,j} - \bar{\phi}_{i-1,j}}{\Delta\bar{x}}\,, \quad \left(\bar{\phi}_{\bar{x}}\right)^{(B)}_{i-1/2,j} = \frac{\bar{\phi}_{i-1,j} - \bar{\phi}_{i-2,j}}{\Delta\bar{x}},$$

and mixed-type difference

$$\left(\bar{\phi}_{\bar{x}}\right)^{(S)}_{i+1/2,j} = \frac{\bar{\phi}_{i+1,j} - \bar{\phi}_{i,j}}{\Delta\bar{x}}\,, \quad \left(\bar{\phi}_{\bar{x}}\right)^{(S)}_{i-1/2,j} = \frac{\bar{\phi}_{i-1,j} - \bar{\phi}_{i-2,j}}{\Delta\bar{x}}.$$

3.1. *Elliptic type*

Equation (11) is elliptic at a point (i, j) when $\chi_{i,j} < 0$. Following Cole & Cook (1986), a central difference method is then applied. We use in (28)

$$\left(\bar{\phi}_{\bar{x}}\right)^{(C)}_{i+1/2,j} - \left(\bar{\phi}_{\bar{x}}\right)^{(C)}_{i-1/2,j} = \frac{1}{\Delta\bar{x}}\left(\bar{\phi}_{i+1,j} - 2\bar{\phi}_{i,j} + \bar{\phi}_{i-1,j}\right),$$

$$\left(\bar{\phi}^2_{\bar{x}}\right)^{(C)}_{i+1/2,j} - \left(\bar{\phi}^2_{\bar{x}}\right)^{(C)}_{i-1/2,j} = \frac{1}{(\Delta\bar{x})^2}\left(\bar{\phi}_{i+1,j} - \bar{\phi}_{i-1,j}\right)\left(\bar{\phi}_{i+1,j} - 2\bar{\phi}_{i,j} + \bar{\phi}_{i-1,j}\right),$$

$$\left(\bar{\phi}^3_{\bar{x}}\right)^{(C)}_{i+1/2,j} - \left(\bar{\phi}^3_{\bar{x}}\right)^{(C)}_{i-1/2,j} = \frac{1}{(\Delta\bar{x})^3}\left(\bar{\phi}_{i+1,j} - 2\bar{\phi}_{i,j} + \bar{\phi}_{i-1,j}\right)\left\{\left(\bar{\phi}_{i+1,j} - \bar{\phi}_{i,j}\right)^2 + \left(\bar{\phi}_{i+1,j} - \bar{\phi}_{i,j}\right)\left(\bar{\phi}_{i,j} - \bar{\phi}_{i-1,j}\right) + \left(\bar{\phi}_{i,j} - \bar{\phi}_{i-1,j}\right)^2\right\},$$

$$\left(\bar{\phi}^4_{\bar{x}}\right)^{(C)}_{i+1/2,j} - \left(\bar{\phi}^4_{\bar{x}}\right)^{(C)}_{i-1/2,j} = \frac{1}{(\Delta\bar{x})^4}\left(\bar{\phi}_{i+1,j} - \bar{\phi}_{i-1,j}\right)\left(\bar{\phi}_{i+1,j} - 2\bar{\phi}_{i,j} + \bar{\phi}_{i-1,j}\right) \times\left\{\left(\bar{\phi}_{i+1,j} - \bar{\phi}_{i,j}\right)^2 + \left(\bar{\phi}_{i,j} - \bar{\phi}_{i-1,j}\right)^2\right\},$$

and

$$\left(\bar{\phi}_{\tilde{y}}\right)^{(C)}_{i,j+1/2} - \left(\bar{\phi}_{\tilde{y}}\right)^{(C)}_{i,j-1/2} = \frac{1}{\Delta\tilde{y}}\left(\bar{\phi}_{i,j+1} - 2\bar{\phi}_{i,j} + \bar{\phi}_{i,j-1}\right).$$

We introduce a stability parameter, $f_{uc} < 0$, for the elliptic-type form of (28):

$$f_{uc\,i,j} \equiv \left\{ -K + K_\Gamma\left(\frac{P1}{\Delta\bar{x}}\right) - \frac{K_A}{3}\left(\frac{(P2)^2 + (P2)(P3) + (P3)^2}{(\Delta\bar{x})^2}\right) + \frac{\Sigma_\infty}{12}\left(\frac{(P1)\left[(P2)^2 + (P3)^2\right]}{(\Delta\bar{x})^3}\right)\right\}, \quad (29)$$

where $P1 = \bar{\phi}_{i+1,j} - \bar{\phi}_{i-1,j}$, $P2 = \bar{\phi}_{i+1,j} - \bar{\phi}_{i,j}$, and $P3 = \bar{\phi}_{i,j} - \bar{\phi}_{i-1,j}$. Therefore, the elliptic-type form of (28) becomes

$$\frac{f_{uci,j}}{(\Delta\bar{x})^2}\left(\bar{\phi}_{i+1,j} - 2\bar{\phi}_{i,j} + \bar{\phi}_{i-1,j}\right) - \frac{1}{(\Delta\tilde{y})^2}\left(\bar{\phi}_{i,j+1} - 2\bar{\phi}_{i,j} + \bar{\phi}_{i,j-1}\right) = 0. \tag{30}$$

For an explicit, point-relaxation solution method, we can compute the velocity potential according to

$$\bar{\phi}_{i,j} = \frac{\dfrac{f_{uci,j}}{(\Delta\bar{x})^2}\left(\bar{\phi}_{i+1,j} + \bar{\phi}_{i-1,j}\right) - \dfrac{1}{(\Delta\tilde{y})^2}\left(\bar{\phi}_{i,j+1} + \bar{\phi}_{i,j-1}\right)}{2\left(\dfrac{f_{uci,j}}{(\Delta\bar{x})^2} - \dfrac{1}{(\Delta\tilde{y})^2}\right)}. \tag{31}$$

Also, from the boundary condition on the airfoil, (30) becomes

$$\frac{f_{uci,j}}{(\Delta\bar{x})^2}\left(\bar{\phi}_{i+1,j} - 2\bar{\phi}_{i,j} + \bar{\phi}_{i-1,j}\right) - \frac{1}{\Delta\tilde{y}}\left(\frac{\bar{\phi}_{i,j+1} - \bar{\phi}_{i,j}}{\Delta\tilde{y}} - \left(\bar{\phi}_{\tilde{y}}\right)_{i,j-1/2}\right) = 0 \tag{32}$$

for $j = 2$, and the velocity potential just above the airfoil at $j = 2$ is

$$\bar{\phi}_{i,2} = \frac{\dfrac{f_{uci,2}}{(\Delta\bar{x})^2}\left(\bar{\phi}_{i+1,2} + \bar{\phi}_{i-1,2}\right) - \dfrac{1}{(\Delta\tilde{y})^2}\left(\bar{\phi}_{i,3} - \left(\bar{\phi}_{\tilde{y}}\right)_{i,3/2}\Delta\tilde{y}\right)}{\dfrac{2f_{uci,2}}{(\Delta\bar{x})^2} - \dfrac{1}{(\Delta\tilde{y})^2}}. \tag{33}$$

Here, as well as in the following sections, $\left(\bar{\phi}_{\tilde{y}}\right)_{i,3/2} = F_u'(\bar{x}_i)$. The potential $\bar{\phi}_{i,1}$ on the airfoil surface is then computed by a second-order linear extrapolation.

For an implicit, line-relaxation solution method (30) becomes

$$\frac{1}{(\Delta\tilde{y})^2}\bar{\phi}_{i,j-1} + 2\left(\frac{f_{uci,j}}{(\Delta\bar{x})^2} - \frac{1}{(\Delta\tilde{y})^2}\right)\bar{\phi}_{i,j} + \frac{1}{(\Delta\tilde{y})^2}\bar{\phi}_{i,j+1} = \frac{f_{uci,j}}{(\Delta\bar{x})^2}\left(\bar{\phi}_{i+1,j} + \bar{\phi}_{i-1,j}\right), \tag{34}$$

and the boundary condition on the airfoil surface is

$$\left(\frac{2f_{uci,2}}{(\Delta\bar{x})^2} - \frac{1}{(\Delta\tilde{y})^2}\right)\bar{\phi}_{i,2} + \frac{1}{(\Delta\tilde{y})^2}\bar{\phi}_{i,3} = \frac{f_{uci,2}}{(\Delta\bar{x})^2}\left(\bar{\phi}_{i+1,2} + \bar{\phi}_{i-1,2}\right) + \frac{1}{\Delta\tilde{y}}\left(\bar{\phi}_{\tilde{y}}\right)_{i,3/2}. \tag{35}$$

3.2. *Hyperbolic type*

Similarly, equation (11) is hyperbolic at a point (i, j) when $\chi_{i,j} > 0$. Following Cole & Cook (1986), a backward difference method is then applied. We use in (28)

$$\left(\bar{\phi}_{\bar{x}}\right)^{(B)}_{i+1/2,j} - \left(\bar{\phi}_{\bar{x}}\right)^{(B)}_{i-1/2,j} = \frac{1}{\Delta\bar{x}}\left(\bar{\phi}_{i,j} - 2\bar{\phi}_{i-1,j} + \bar{\phi}_{i-2,j}\right),$$

$$\left(\bar{\phi}^2_{\bar{x}}\right)^{(B)}_{i+1/2,j} - \left(\bar{\phi}^2_{\bar{x}}\right)^{(B)}_{i-1/2,j} = \frac{1}{(\Delta\bar{x})^2}\left(\bar{\phi}_{i,j} - \bar{\phi}_{i-2,j}\right)\left(\bar{\phi}_{i,j} - 2\bar{\phi}_{i-1,j} + \bar{\phi}_{i-2,j}\right),$$

$$\left(\bar{\phi}^3_{\bar{x}}\right)^{(B)}_{i+1/2,j} - \left(\bar{\phi}^3_{\bar{x}}\right)^{(B)}_{i-1/2,j} = \frac{1}{(\Delta\bar{x})^3}\left(\bar{\phi}_{i,j} - 2\bar{\phi}_{i-1,j} + \bar{\phi}_{i-2,j}\right)\left\{\left(\bar{\phi}_{i,j} - \bar{\phi}_{i-1,j}\right)^2 + \left(\bar{\phi}_{i,j} - \bar{\phi}_{i-1,j}\right)\left(\bar{\phi}_{i-1,j} - \bar{\phi}_{i-2,j}\right) + \left(\bar{\phi}_{i-1,j} - \bar{\phi}_{i-2,j}\right)^2\right\},$$

$$\left(\bar{\phi}^4_{\bar{x}}\right)^{(B)}_{i+1/2,j} - \left(\bar{\phi}^4_{\bar{x}}\right)^{(B)}_{i-1/2,j} = \frac{1}{(\Delta\bar{x})^4}\left(\bar{\phi}_{i,j} - \bar{\phi}_{i-2,j}\right)\left(\bar{\phi}_{i,j} - 2\bar{\phi}_{i-1,j} + \bar{\phi}_{i-2,j}\right)$$
$$\times\left\{\left(\bar{\phi}_{i,j} - \bar{\phi}_{i-1,j}\right)^2 + \left(\bar{\phi}_{i-1,j} - \bar{\phi}_{i-2,j}\right)^2\right\}.$$

Another stability parameter, $f_{ub} > 0$, for a hyperbolic-type form of (28) is

$$f_{ub\,i,j} \equiv \left\{ -K + K_\Gamma\left(\frac{P4}{\Delta\bar{x}}\right) - \frac{K_\Lambda}{3}\left(\frac{(P3)^2 + (P3)(P5) + (P5)^2}{(\Delta\bar{x})^2}\right) + \frac{\Sigma_\infty}{12}\left(\frac{(P4)\left[(P3)^2 + (P5)^2\right]}{(\Delta\bar{x})^3}\right)\right\}, \quad (36)$$

where $P4 = \bar{\phi}_{i,j} - \bar{\phi}_{i-2,j}$, $P5 = \bar{\phi}_{i-1,j} - \bar{\phi}_{i-2,j}$, and $P3$ is defined in the previous subsection. So, the hyperbolic-type form of (28) becomes

$$\frac{f_{ub\,i,j}}{(\Delta\bar{x})^2}\left(\bar{\phi}_{i,j} - 2\bar{\phi}_{i-1,j} + \bar{\phi}_{i-2,j}\right) - \frac{1}{(\Delta\tilde{y})^2}\left(\bar{\phi}_{i,j+1} - 2\bar{\phi}_{i,j} + \bar{\phi}_{i,j-1}\right) = 0. \quad (37)$$

For an explicit, point-relaxation solution method, we compute the velocity potential from

$$\bar{\phi}_{i,j} = \frac{\dfrac{f_{ub\,i,j}}{(\Delta\bar{x})^2}\left(2\bar{\phi}_{i-1,j} - \bar{\phi}_{i-2,j}\right) - \dfrac{1}{(\Delta\tilde{y})^2}\left(\bar{\phi}_{i,j+1} + \bar{\phi}_{i,j-1}\right)}{\dfrac{f_{ub\,i,j}}{(\Delta\bar{x})^2} + \dfrac{2}{(\Delta\tilde{y})^2}}. \quad (38)$$

The boundary condition on the airfoil becomes

$$\frac{f_{ub\,i,j}}{(\Delta\bar{x})^2}\left(\bar{\phi}_{i,j} - 2\bar{\phi}_{i-1,j} + \bar{\phi}_{i-2,j}\right) - \frac{1}{\Delta\tilde{y}}\left(\frac{\bar{\phi}_{i,j+1} - \bar{\phi}_{i,j}}{\Delta\tilde{y}} - \left(\bar{\phi}_{\tilde{y}}\right)_{i,j-1/2}\right) = 0 \quad (39)$$

for $j = 2$, and the velocity potential just above the airfoil is

$$\bar{\phi}_{i,2} = \frac{\dfrac{f_{ub\,i,2}}{(\Delta\bar{x})^2}\left(2\bar{\phi}_{i-1,2} - \bar{\phi}_{i-2,2}\right) - \dfrac{1}{(\Delta\tilde{y})^2}\left(\bar{\phi}_{i,3} - \left(\bar{\phi}_{\tilde{y}}\right)_{i,3/2}\Delta\tilde{y}\right)}{\dfrac{f_{ub\,i,2}}{(\Delta\bar{x})^2} + \dfrac{1}{(\Delta\tilde{y})^2}}. \quad (40)$$

The potential $\bar{\phi}_{i,1}$ on the airfoil surface is then computed by a second-order linear extrapolation.

For an implicit, line-relaxation solution method (37) becomes

$$\frac{1}{(\Delta\tilde{y})^2}\bar{\phi}_{i,j-1} - \left(\frac{f_{ub\,i,j}}{(\Delta\bar{x})^2} + \frac{2}{(\Delta\tilde{y})^2}\right)\bar{\phi}_{i,j} + \frac{1}{(\Delta\tilde{y})^2}\bar{\phi}_{i,j+1} = \frac{f_{ub\,i,j}}{(\Delta\bar{x})^2}\left(-2\bar{\phi}_{i-1,j} + \bar{\phi}_{i-2,j}\right), \quad (41)$$

and the boundary condition on the airfoil surface is

$$-\left(\frac{f_{ub\,i,2}}{(\Delta\bar{x})^2} + \frac{1}{(\Delta\tilde{y})^2}\right)\bar{\phi}_{i,2} + \frac{1}{(\Delta\tilde{y})^2}\bar{\phi}_{i,3} = \frac{f_{ub\,i,2}}{(\Delta\bar{x})^2}\left(-2\bar{\phi}_{i-1,2} + \bar{\phi}_{i-2,2}\right) + \frac{1}{\Delta\tilde{y}}\left(\bar{\phi}_{\tilde{y}}\right)_{i,3/2}. \quad (42)$$

3.3. *Shock type*

We expect a mixed-type form of (11) when a shock wave may appear in the flow. The flow is supersonic ahead of the shock wave, where a backward difference method is applied, and is subsonic behind the shock wave, where a central difference method is

applied. We use in (28)

$$\left(\bar{\phi}_{\bar{x}}\right)^{(S)}_{i+1/2,j} - \left(\bar{\phi}_{\bar{x}}\right)^{(S)}_{i-1/2,j} = \frac{1}{\Delta\bar{x}}\left(\bar{\phi}_{i+1,j} - \bar{\phi}_{i,j} - \bar{\phi}_{i-1,j} + \bar{\phi}_{i-2,j}\right),$$

$$\left(\bar{\phi}^2_{\bar{x}}\right)^{(S)}_{i+1/2,j} - \left(\bar{\phi}^2_{\bar{x}}\right)^{(S)}_{i-1/2,j} = \frac{1}{(\Delta\bar{x})^2}\left(\bar{\phi}_{i+1,j} - \bar{\phi}_{i,j} - \bar{\phi}_{i-1,j} + \bar{\phi}_{i-2,j}\right) \times \left(\bar{\phi}_{i+1,j} - \bar{\phi}_{i,j} + \bar{\phi}_{i-1,j} - \bar{\phi}_{i-2,j}\right),$$

$$\left(\bar{\phi}^3_{\bar{x}}\right)^{(S)}_{i+1/2,j} - \left(\bar{\phi}^3_{\bar{x}}\right)^{(S)}_{i-1/2,j} = \frac{1}{(\Delta\bar{x})^3}\left(\bar{\phi}_{i+1,j} - \bar{\phi}_{i,j} - \bar{\phi}_{i-1,j} + \bar{\phi}_{i-2,j}\right)\left\{\left(\bar{\phi}_{i+1,j} - \bar{\phi}_{i,j}\right)^2 + \left(\bar{\phi}_{i+1,j} - \bar{\phi}_{i,j}\right)\left(\bar{\phi}_{i-1,j} - \bar{\phi}_{i-2,j}\right) + \left(\bar{\phi}_{i-1,j} - \bar{\phi}_{i-2,j}\right)^2\right\},$$

$$\left(\bar{\phi}^4_{\bar{x}}\right)^{(S)}_{i+1/2,j} - \left(\bar{\phi}^4_{\bar{x}}\right)^{(S)}_{i-1/2,j} = \frac{1}{(\Delta\bar{x})^4}\left(\bar{\phi}_{i+1,j} - \bar{\phi}_{i,j} - \bar{\phi}_{i-1,j} + \bar{\phi}_{i-2,j}\right) \times \left(\bar{\phi}_{i+1,j} - \bar{\phi}_{i,j} + \bar{\phi}_{i-1,j} - \bar{\phi}_{i-2,j}\right)\left\{\left(\bar{\phi}_{i+1,j} - \bar{\phi}_{i,j}\right)^2 + \left(\bar{\phi}_{i-1,j} - \bar{\phi}_{i-2,j}\right)^2\right\}.$$

Let f_{us} be

$$f_{usi,j} \equiv \left\{ -K + K_\Gamma\left(\frac{P2+P5}{\Delta\bar{x}}\right) - \frac{K_\Lambda}{3}\left(\frac{(P2)^2 + (P2)(P5) + (P5)^2}{(\Delta\bar{x})^2}\right) + \frac{\Sigma_\infty}{12}\left(\frac{(P2+P5)\left[(P2)^2 + (P5)^2\right]}{(\Delta\bar{x})^3}\right)\right\}, \tag{43}$$

where $P2$ and $P5$ are defined in previous subsections. Therefore, for a mixed-type form of (28) we have

$$\frac{f_{usi,j}}{(\Delta\bar{x})^2}\left(\bar{\phi}_{i+1,j} - \bar{\phi}_{i,j} - \bar{\phi}_{i-1,j} + \bar{\phi}_{i-2,j}\right) - \frac{1}{(\Delta\tilde{y})^2}\left(\bar{\phi}_{i,j+1} - 2\bar{\phi}_{i,j} + \bar{\phi}_{i,j-1}\right) = 0. \tag{44}$$

For an explicit, point-relaxation solution method, we can compute the velocity potential at a shock wave point from

$$\bar{\phi}_{i,j} = \frac{\dfrac{f_{usi,j}}{(\Delta\bar{x})^2}\left(\bar{\phi}_{i+1,j} - \bar{\phi}_{i-1,j} + \bar{\phi}_{i-2,j}\right) - \dfrac{1}{(\Delta\tilde{y})^2}\left(\bar{\phi}_{i,j+1} + \bar{\phi}_{i,j-1}\right)}{\left(\dfrac{f_{usi,j}}{(\Delta\bar{x})^2} - \dfrac{2}{(\Delta\tilde{y})^2}\right)}. \tag{45}$$

The boundary condition on the airfoil surface becomes

$$\frac{f_{usi,j}}{(\Delta\bar{x})^2}\left(\bar{\phi}_{i+1,j} - \bar{\phi}_{i,j} - \bar{\phi}_{i-1,j} + \bar{\phi}_{i-2,j}\right) - \frac{1}{\Delta\tilde{y}}\left(\frac{\bar{\phi}_{i,j+1} - \bar{\phi}_{i,j}}{\Delta\tilde{y}} - \left(\bar{\phi}_{\tilde{y}}\right)_{i,j-1/2}\right) = 0 \tag{46}$$

for $j = 2$, and the velocity potential just above the airfoil is

$$\bar{\phi}_{i,2} = \frac{\dfrac{f_{usi,2}}{(\Delta\bar{x})^2}\left(\bar{\phi}_{i+1,2} - \bar{\phi}_{i-1,2} + \bar{\phi}_{i-2,2}\right) - \dfrac{1}{(\Delta\tilde{y})^2}\left(\bar{\phi}_{i,3} - \left(\bar{\phi}_{\tilde{y}}\right)_{i,3/2}\Delta\tilde{y}\right)}{\dfrac{f_{usi,2}}{(\Delta\bar{x})^2} - \dfrac{1}{(\Delta\tilde{y})^2}}. \tag{47}$$

The potential $\bar{\phi}_{i,1}$ on the airfoil surface is computed by a second-order linear extrapolation.

For an implicit, line-relaxation solution method (44) becomes

$$\frac{1}{(\Delta\tilde{y})^2}\bar{\phi}_{i,j-1}+\left(\frac{f_{usi,j}}{(\Delta\bar{x})^2}-\frac{2}{(\Delta\tilde{y})^2}\right)\bar{\phi}_{i,j}+\frac{1}{(\Delta\tilde{y})^2}\bar{\phi}_{i,j+1} = \frac{f_{usi,j}}{(\Delta\bar{x})^2}\left(\bar{\phi}_{i+1,j}-\bar{\phi}_{i-1,j}+\bar{\phi}_{i-2,j}\right), \tag{48}$$

and the boundary condition on the airfoil surface is

$$\left(\frac{f_{usi,2}}{(\Delta\bar{x})^2}-\frac{1}{(\Delta\tilde{y})^2}\right)\bar{\phi}_{i,2}+\frac{1}{(\Delta\tilde{y})^2}\bar{\phi}_{i,3} = \frac{f_{usi,2}}{(\Delta\bar{x})^2}\left(\bar{\phi}_{i+1,2}-\bar{\phi}_{i-1,2}+\bar{\phi}_{i-2,2}\right)+\frac{1}{\Delta\tilde{y}}\left(\bar{\phi}_{\tilde{y}}\right)_{i,3/2}. \tag{49}$$

3.4. *Sonic type*

At a sonic point where $\chi_{i,j}=0$, equation (11) is parabolic. Unlike a shock point, the flow in the neighbourhood of a sonic point is continuous, subsonic ahead and supersonic behind it. Thus, a central difference method is used ahead of a sonic point and a backward difference method behind it. Equation (28) becomes

$$\left(\bar{\phi}_{\bar{x}}\right)_{i+1/2,j}-\left(\bar{\phi}_{\bar{x}}\right)_{i-1/2,j}=0,$$

or

$$\frac{\bar{\phi}_{i,j+1}-2\bar{\phi}_{i,j}+\bar{\phi}_{i,j-1}}{(\Delta\tilde{y})^2}=0. \tag{50}$$

For an explicit, point-relaxation solution method, the velocity potential at this sonic point is

$$\bar{\phi}_{i,j}=\frac{\bar{\phi}_{i,j+1}+\bar{\phi}_{i,j-1}}{2}, \tag{51}$$

and the boundary condition on the airfoil is described by

$$\bar{\phi}_{i,2}=\bar{\phi}_{i,3}-\left(\bar{\phi}_{\tilde{y}}\right)_{i,3/2}\Delta\tilde{y}. \tag{52}$$

The potential $\bar{\phi}_{i,1}$ on the airfoil surface is computed by a second-order linear extrapolation.

For an implicit, line-relaxation solution method (50) becomes

$$\bar{\phi}_{i,j-1}-2\bar{\phi}_{i,j}+\bar{\phi}_{i,j+1}=0, \tag{53}$$

and the boundary condition on the airfoil surface is

$$\bar{\phi}_{i,3}-\bar{\phi}_{i,2}=\left(\bar{\phi}_{\tilde{y}}\right)_{i,3/2}\Delta\tilde{y} \tag{54}$$

3.5. *The algorithm of the solution*

For a symmetric airfoil at zero angle of attack, a computational domain in the upper half of the flow field and a rectangular mesh with equal spacing in $\bar{x}$ and $\tilde{y}$ are used. Since the disturbances are created by the existence of the airfoil, a study of the size of the computational domain suggests that the far-field boundary condition, $\bar{\phi}=0$, has a small effect on the solution. Therefore, a relatively small computational domain may be used. For a small control volume, the far-field boundary condition of $\bar{\phi}$ at the inlet, outlet, and upper sections of the domain cannot be fixed. For the continuity

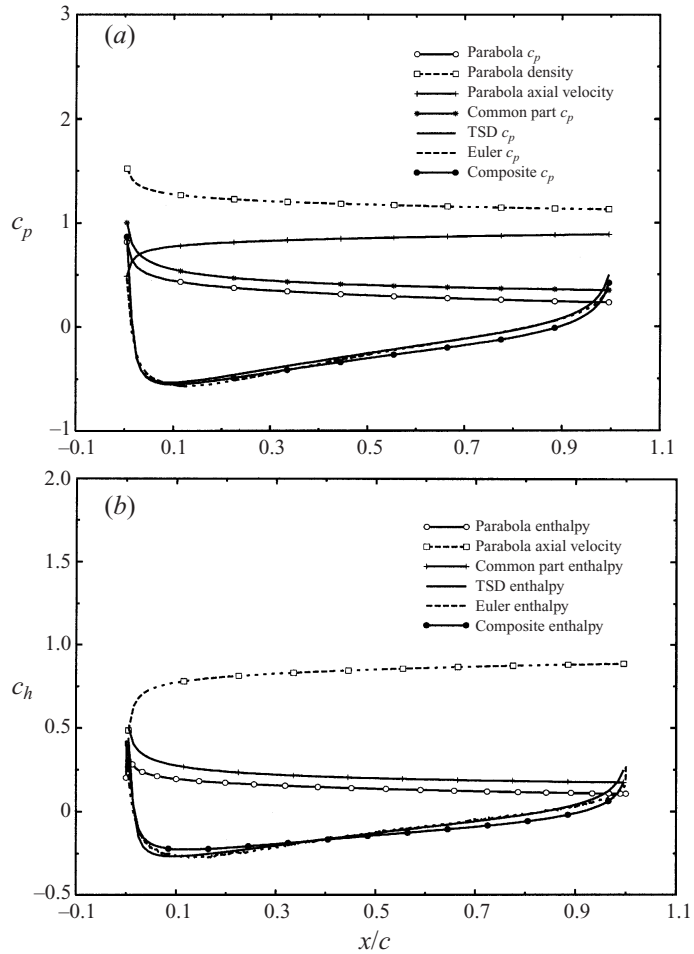

FIGURE 3. The subsonic case: comparison of (*a*) pressure coefficient distributions and (*b*) specific enthalpy distributions, along a NACA0006 airfoil.

of the flow, the solution on these computational domain boundaries is extrapolated from inside the computational domain. The boundary condition along the airfoil uses the above equations according to the type of equation at the point. A symmetry condition is imposed along the x-axis ahead of and behind the airfoil.

An explicit, point-relaxation method is used to compute the potential $\bar{\phi}$. At the initial time step, zero values of disturbances are given for the entire computational domain. Following Cole & Cook (1986), the code evaluates the type of governing equation at each grid point according to the following criteria:

$$\begin{aligned} \text{elliptic point when} \quad & f_{uci,j} < 0 \ \text{ and } \ f_{ubi,j} < 0, \\ \text{hyperbolic point when} \quad & f_{uci,j} > 0 \ \text{ and } \ f_{ubi,j} > 0, \\ \text{sonic point when} \quad & f_{uci,j} > 0 \ \text{ and } \ f_{ubi,j} < 0, \\ \text{shock point when} \quad & f_{uci,j} < 0 \ \text{ and } \ f_{ubi,j} > 0. \end{aligned}$$

After the type of the governing equation is identified at each point, equations (30), (32) or (37), (39) or (44), (46) or (51), (52) are used to compute the velocity potential

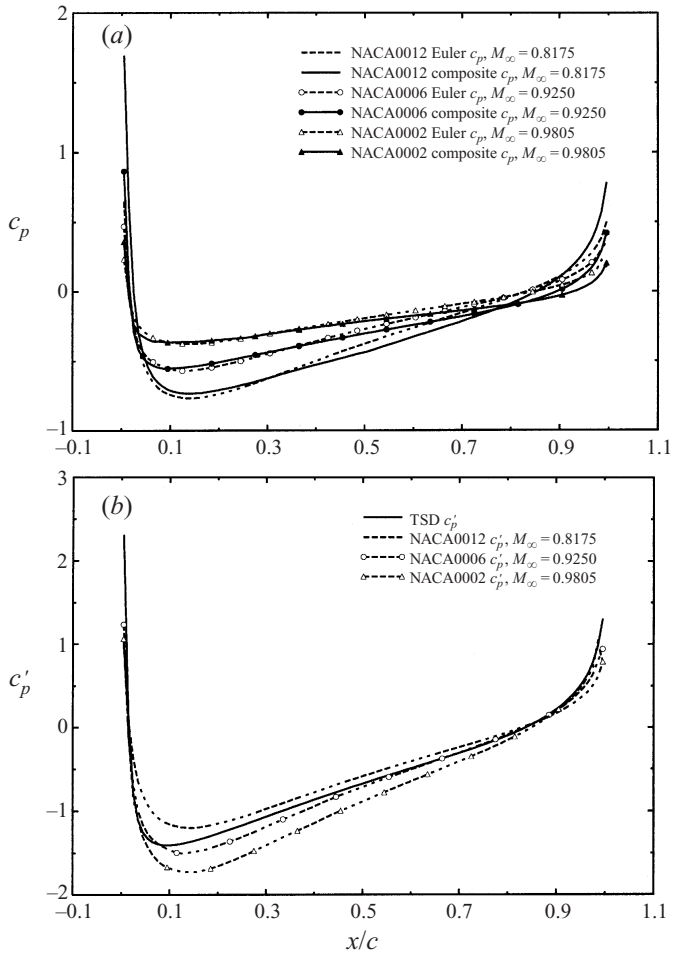

FIGURE 4. The subsonic case. (*a*) Comparison of pressure coefficient distributions according to the Euler solutions and the theoretical composite solutions. (*b*) Comparison of the similarity rules in pressure coefficient distributions between the Euler solutions and the TSD solution.

at this point. The updated value of the potential is used for the computation of next point. The maximum of the absolute change of the potential at each time step in the entire domain indicates convergence to the steady state. Iterations are repeated until the maximum of the absolute change is less than 10^{-6}. The pressure coefficient at every point is then computed from the changes of velocity potential according to $c_{pTSD} = -2\epsilon^{2/5}\bar{\phi}_{1\bar{x}}$.

4. Numerical studies

The TSD equation solver has been verified in Wang (1998) for several cases by first studying transonic flow of perfect gas around a NACA airfoil. Then, a mesh convergence study was conducted with various meshes and computational domain sizes. Refining the mesh in both the $\bar{x}$- and $\tilde{y}$-directions results in mesh-converged numerical solutions; however, more computational iterations are needed to achieve such solutions. Computational domains of various sizes have been studied with non-

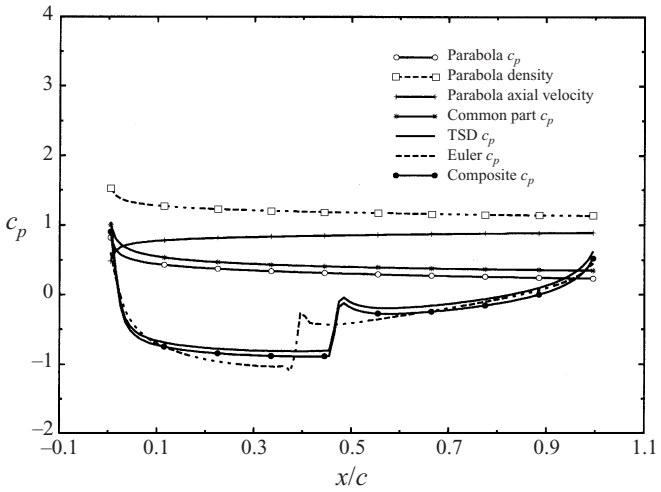

FIGURE 5. The transonic case: comparison of pressure coefficient distributions along a NACA0006 airfoil.

reflecting boundary conditions on the outer boundaries (Wang 1998). It is found that a domain of 3c by 1.5c with a 300 by 800 mesh results, after about 40 000 iterations, in a converged solution and is used for computing the cases discussed in the following subsections.

All results presented here are computed using the van der Waals equation of state. The Appendix provides formulas for computing the thermodynamic properties, Γ, Λ, and Σ of the van der Waals gas, based on the pressure and density. In the following examples, a BZT gas with $R/c_v = 0.02$ is used.

In the first examples, we concentrate on the BZT gas with the properties $\Gamma_\infty = \Lambda_\infty = 0$ and $\Sigma_\infty = 16.05$ for which $p_\infty/p_c = 1.0696$ and $\rho_\infty/\rho_c = 0.735$. Subsonic, transonic, and sonic flows around three NACA airfoils at zero angle of attack with thickness ratios of 0.12, 0.06, and 0.02 are computed. The TSD solutions in the outer region are computed using the TSD equation solver. Then, the inner parabola problem is solved by the Euler solver of Morren (1990). See also Rusak & Wang (1997) for details of the inner problem solution. Using the TSD solution and the parabola solution, the composite solutions for the pressure coefficient and the specific enthalpy are computed according to the analytical formulas (22) and (24). Results of the composite solution are compared in each case with the numerical solution of the Euler equations using Morren's (1990) code.

4.1. *Subsonic case*

In this case, a similarity parameter $K = 4.22$ is used. Therefore, we have $M_\infty = 0.8175$ for the flow around a NACA0012, $M_\infty = 0.9250$ for the flow around a NACA0006, and $M_\infty = 0.9805$ for the flow around a NACA0002. In all of these cases, the flows are of subsonic nature. Figure 3(*a*) shows an example of the details that are needed to compute the composite solutions for the pressure coefficient along the NACA0006 surface. In this figure, as well as later in figures 3(*b*), 5, 7 and 13, we present the TSD solution, the parabola solution for pressure, density, and axial velocity, the common part, the composite solution, and the Euler solution. It can be seen from figure 3(*a*) that the composite solution predicts the Euler solution, specifically near the nose of the airfoil and the minimum suction point. Solutions deviate a little after the mid-

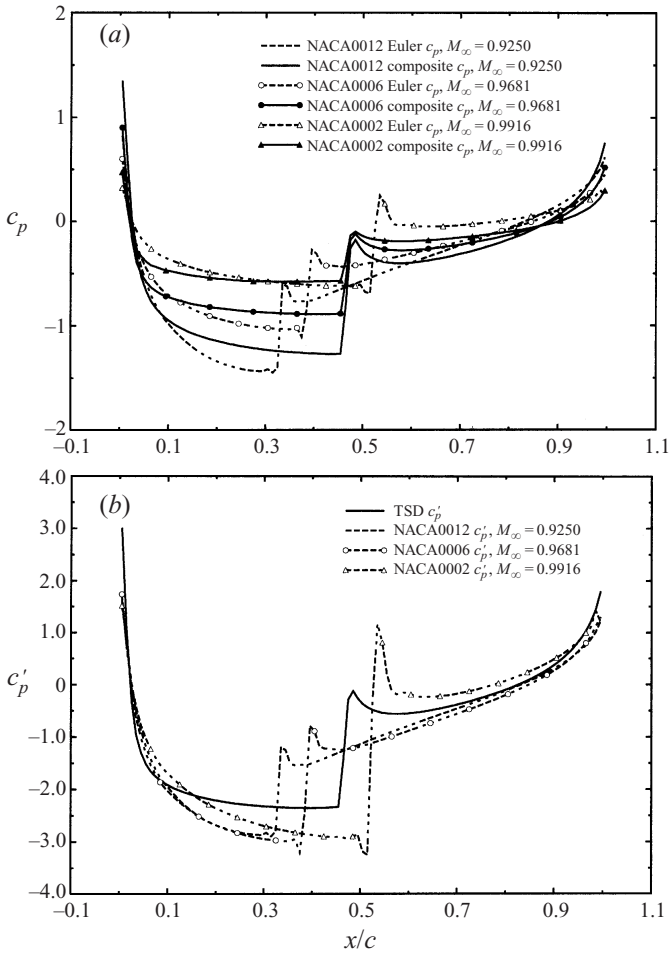

FIGURE 6. The transonic case. (*a*) Comparison of pressure coefficient distributions between Euler solutions and theoretical composite solutions. (*b*) Comparison of the similarity rules in pressure coefficient distributions between Euler solutions and TSD solution.

airfoil position and this may be related to the higher-order effects, of $O(\epsilon^{4/5}, 1 - M_\infty^2)$, that are not included in the composite solution.

Figure 3(*b*) shows an example of the details that are needed to compute the composite solution for the specific enthalpy along the NACA0006 airfoil surface. It can be seen that the specific enthalpy also nicely predicts the Euler solution.

Figure 4(*a*) summarizes the comparison between the composite solutions and the Euler solutions for the three cases where $K = 4.22$ and $K_\Gamma = K_\Lambda = 0$. The self-similar behaviour between the flow cases is evident, specifically at the points where $c_p = 0$ and at the minimum suction point.

In order to demonstrate the self-similarity between the flow cases for $K = 4.22$, the Euler solutions for the rescaled pressure coefficient, $c_p' = c_p/\epsilon^{2/5}$, are presented in figure 4(*b*). Also shown in this figure is the TSD result for $c_p' = -2\bar{\phi}_{\bar{x}}$. Results show that in this magnified scale of c_p, the TSD result is the dominant term of c_p, except near the leading edge where the parabola solution dominates. As mentioned above, the deviations from an exact self-similar behaviour between the cases may be due to second-order nonlinear effects that are neglected in the TSD theory but appear in

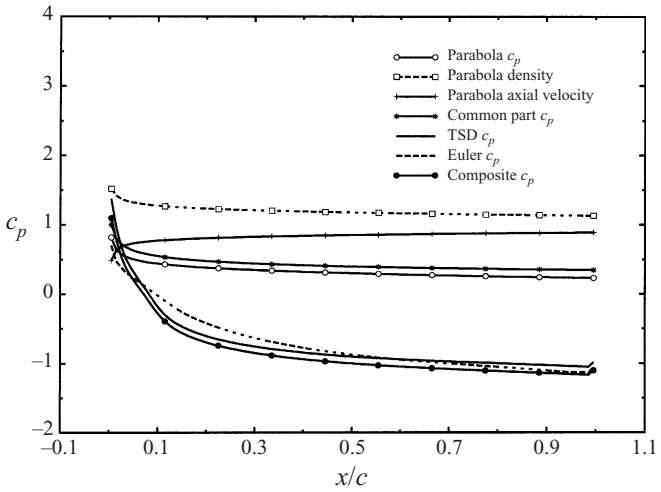

FIGURE 7. The sonic case: comparison of pressure coefficient distributions along a NACA0006 airfoil.

solutions of (1). These can amount to local relative errors on the order of 20–30% when the scaled pressure coefficient is computed, specifically when $\epsilon = 0.12$ and near the point of maximum suction.

4.2. *Transonic case*

In this case, a similarity parameter $K = 1.84$ is used. Therefore, we have $M_\infty = 0.9250$ for the flow around a NACA0012, $M_\infty = 0.9681$ for the flow around a NACA0006, and $M_\infty = 0.9916$ for the flow around a NACA0002. In all of these cases, the flows are of transonic nature with a compression shock wave near the middle of the airfoil's chord. Figure 5 shows an example of the details that are needed to compute the composite solution for the pressure coefficient along the NACA0006 surface. It can be seen that the composite solutions predict the flow behaviour near the airfoil's nose and trailing edge as well as the appearance of the shock wave at about 40% of the airfoil's chord. The composite solution deviates from the numerical Euler solution, specifically at the shock wave position (deviation of about 6% of the airfoil's chord) and around it. This may be related to the small entropy production behind the shock wave that is not included in the composite, or TSD, solution but appears in the solution of (1).

Figure 6(*a*) summarizes the comparison between the composite solutions and the Euler solutions for the three cases where $K = 1.84$ and $K_\Gamma = K_\Lambda = 0$. The self-similar behaviour between the flow cases is evident, specifically at the points where $c_p = 0$. Again, the deviation in the shock wave positions may be explained by the entropy production behind the shock wave. Note that this deviation becomes smaller as ϵ is reduced.

In order to demonstrate the self-similarity between the flow cases for $K = 1.84$, the Euler solutions for the rescaled pressure coefficient, $c_p' = c_p/\epsilon^{2/5}$, are presented in figure 6(*b*). Also shown in this figure is the TSD result for $c_p' = -2\bar{\phi}_{\bar{x}}$. Results show that in this magnified scale of c_p, the TSD result is the dominant term of c_p, except near the airfoil's leading edge. The deviations from an exact self-similar behaviour between the cases may be due to the coupling between the entropy production behind the shock waves and the second-order nonlinear effects that are both neglected in the

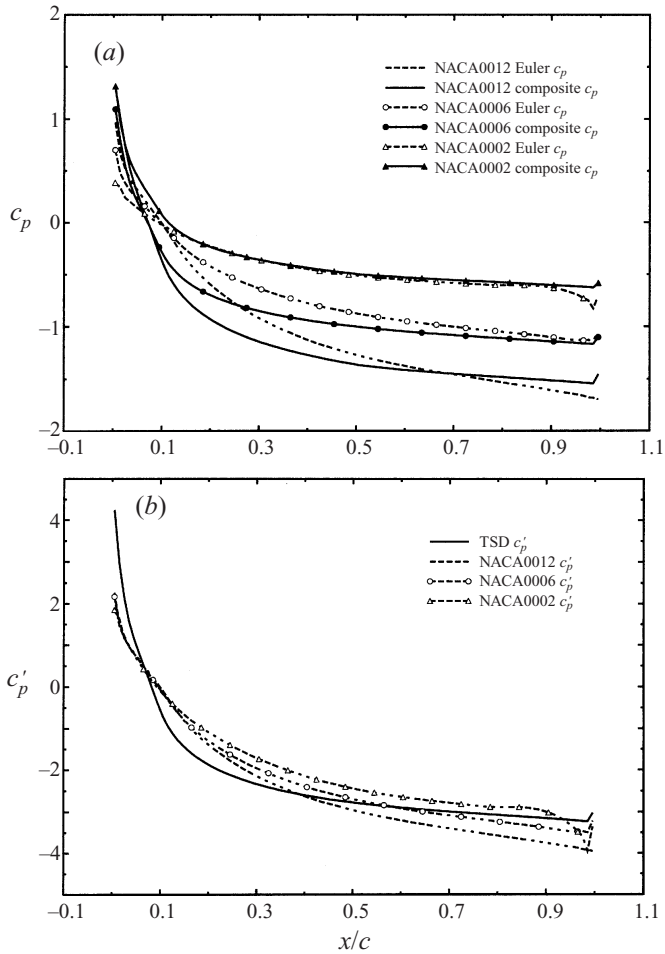

FIGURE 8. The sonic case. (*a*) Comparison of pressure coefficient distributions between Euler solutions and theoretical composite solutions. (*b*) Comparison of the similarity rules in pressure coefficient distributions between Euler solutions and TSD solution.

TSD theory but appear in solutions of (1). In computing the scaled pressure, these may amount together to a local relative error of 30% near the maximum thickness point of the airfoil.

4.3. *Sonic case*

In this case, a similarity parameter $K = 0.0025$ is used. Therefore, we have $M_\infty = 0.9999$ for the flows around the three NACA airfoils. In all of these cases, the flows are of sonic nature with a relatively strong tail shock wave at the trailing edge of the airfoil. Figure 7 shows an example of the details that are needed to compute the composite solution for the pressure coefficient along the NACA0006 surface. It can be seen that the composite solution predicts the Euler solution, specifically near the nose of the airfoil and the minimum suction level near the trailing edge. The solution deviates near the middle of the airfoil. This may be related to the higher order effects of $O(\epsilon^{4/5})$ that are not included in the composite, or TSD, solution.

Figure 8(*a*) summarizes the comparison between the composite solutions and the

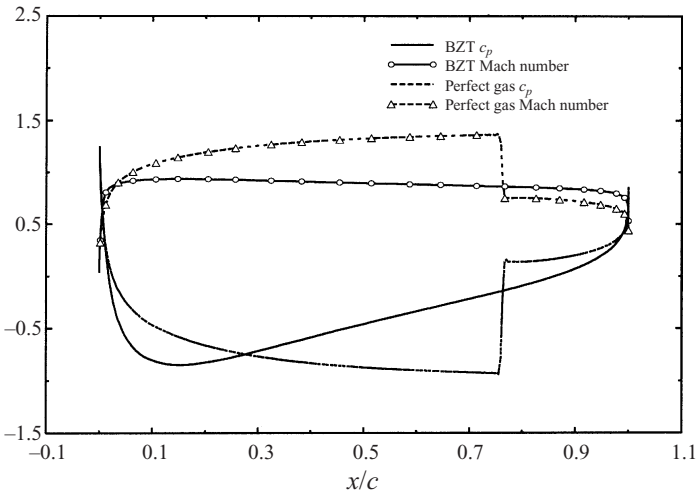

FIGURE 9. A comparison of Mach number and pressure coefficient distributions between a BZT gas flow and a perfect gas flow around a NACA0012 airfoil with the same $M_\infty = 0.85$.

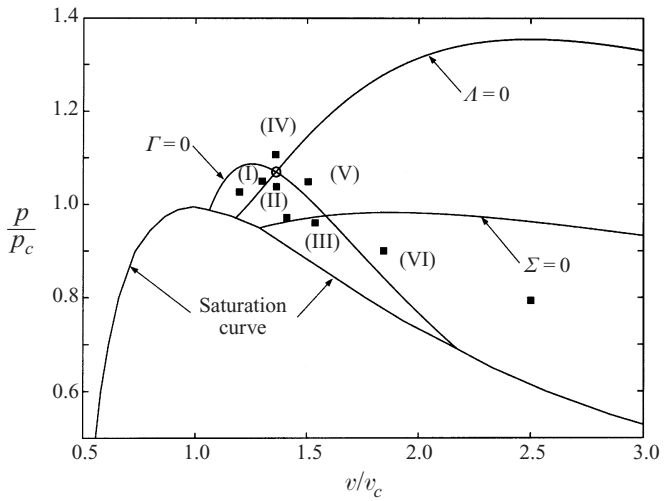

FIGURE 10. The map of Γ, Λ and Σ for a van der Waals gas with $R/c_v = 0.02$.

Zone number	Γ	Λ	Σ
I	—	+	+
II	—	—	+
III	—	—	—
IV	+	+	+
V	+	—	+
VI	+	—	—

TABLE 1. The signs of Γ, Λ and Σ in various zones.

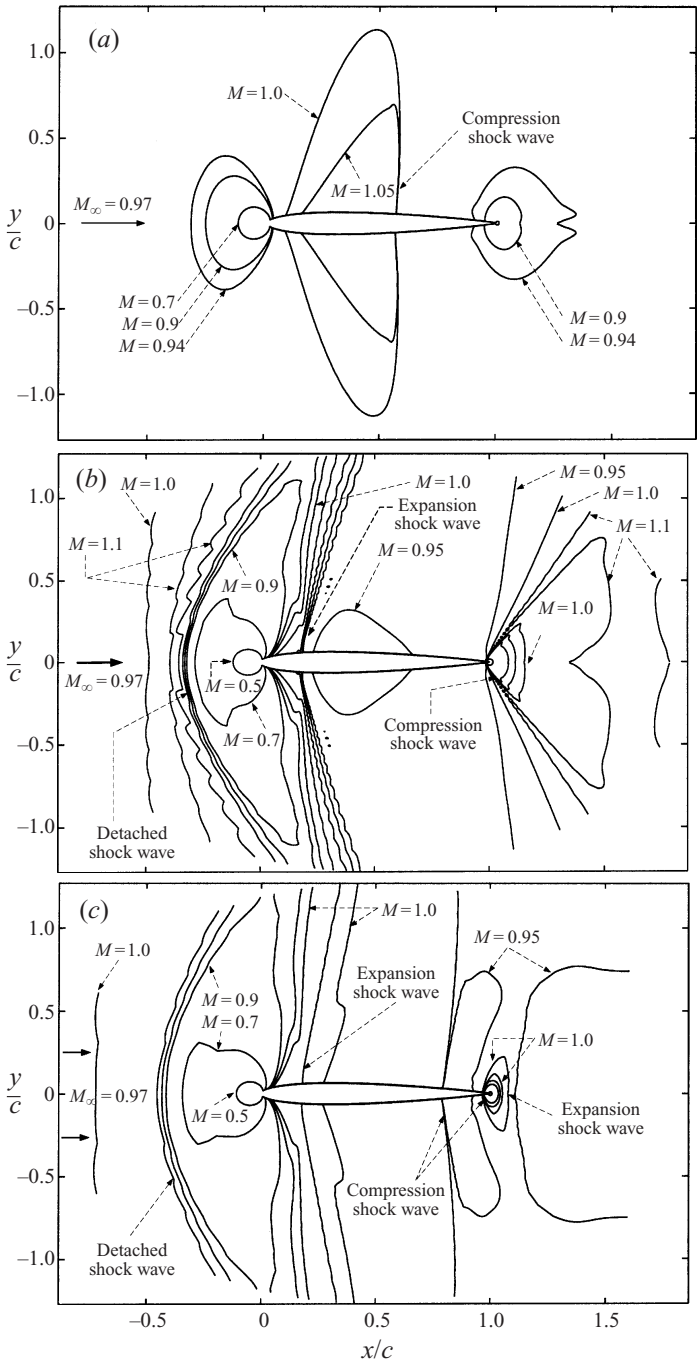

FIGURE 11 (*a–c*). For caption see facing page.

Euler solutions for the three cases where $K = K_\Gamma = K_A = 0$. It can be seen that the solution accuracy improves as ϵ is reduced.

In order to demonstrate the self-similarity between the flow cases for $K = 0$, the Euler solutions for the rescaled pressure coefficient, $c'_p = c_p/\epsilon^{2/5}$, are presented in figure 8(*b*). Also shown in this figure is the TSD result for $c'_p = -2\bar{\phi}_{\bar{x}}$. Results show

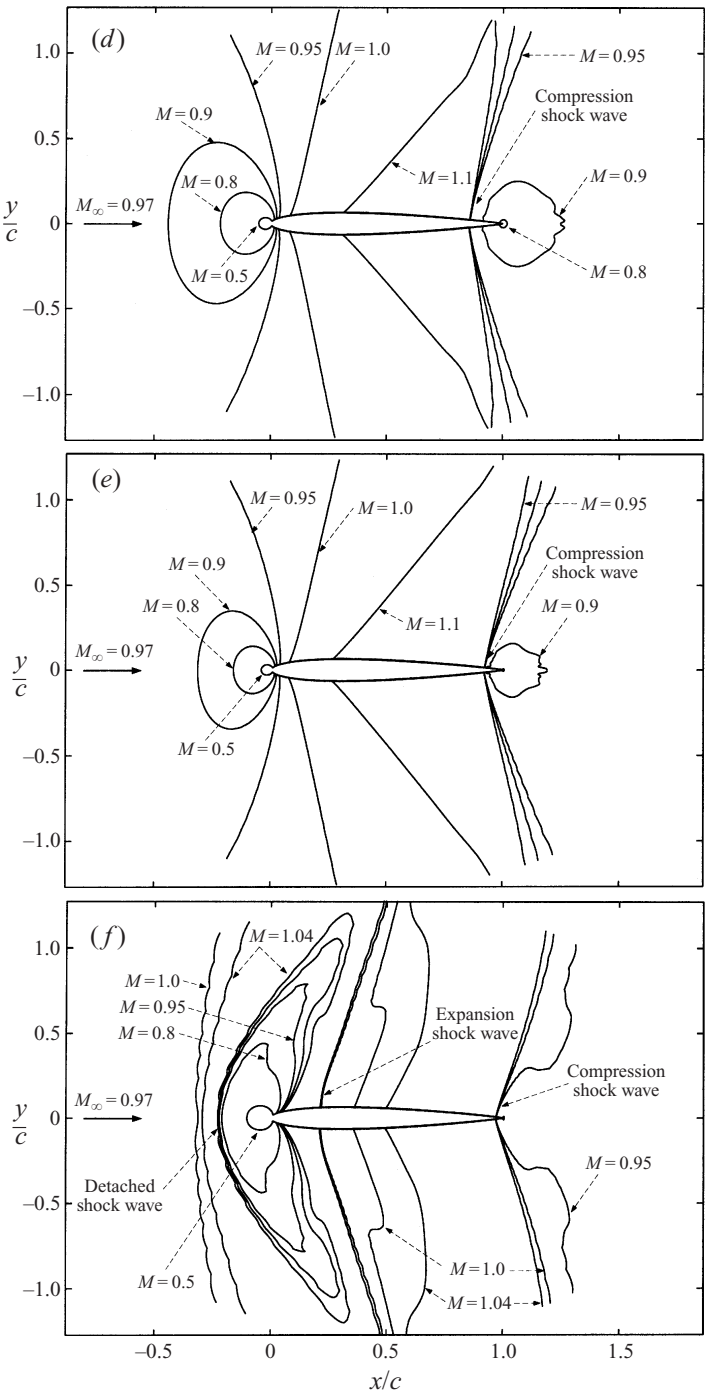

FIGURE 11. Mach number contour plots for a BZT gas flow with $R/c_v = 0.02$ around a NACA0012 airfoil at $M_\infty = 0.97$: (*a*) zone I: $p/p_c = 1.06$, $v/v_c = 1.13$; (*b*) zone II: $p/p_c = 0.97$, $v/v_c = 1.42$; (*c*) zone III: $p/p_c = 0.96$, $v/v_c = 1.55$; (*d*) zone IV: $p/p_c = 1.10$, $v/v_c = 1.36$; (*e*) zone V: $p/p_c = 1.05$, $v/v_c = 1.50$; (*f*) zone IV: $p/p_c = 0.90$, $v/v_c = 1.75$.

that in this magnified scale of c_p, the TSD result is the dominant term of c_p, except near the airfoil's leading edge. As in the transonic case, the deviations from an exact self-similar behaviour between the cases may result from the strong coupling between the entropy production behind the shock waves and the second-order nonlinear effects that are both neglected in the TSD theory but appear in the solutions of (1). In computing the scaled pressure, these may amount together to a local relative error of about 50% near the leading edge of the airfoil.

4.4. *The flow patterns in transonic flow of BZT gases*

The computational results presented in the previous subsections are computed for a BZT gas characterized by $\Gamma_\infty = \Lambda_\infty = 0$ for which $p_\infty/p_c = 1.07$ and $v_\infty/v_c = 1.36$. The flow patterns of the above cases are similar to those of a perfect gas in subsonic, transonic, and sonic flows. However, the critical Mach number of the BZT gas is much higher than that of perfect gas. Figure 9 shows the pressure coefficients along a NACA0012 airfoil in an oncoming flow with $M_\infty = 0.85$ according to solutions of (1). The BZT gas flow has not yet encountered any flow discontinuity on the airfoil as the perfect gas did. It is demonstrated that the BZT gas flow tends to have less pressure drag at the same M_∞. Similar behaviour was also found by Tarkenton & Cramer (1993). Actually, the critical Mach number for NACA0012 at zero angle of attack is 0.74 when it operates in a perfect gas (see Kuethe & Chow 1986) and it is 0.88 when it operates in a BZT gas at $\Gamma_\infty = \Lambda_\infty = 0$.

From all the BZT gas flow cases that are described in the following, it seems that the flow pattern of a BZT gas changes not only with the flow speed (or M_∞), but also with the values of Γ_∞, Λ_∞ and Σ_∞. The values of Γ, Λ, Σ, p and v in the following discussion represent the upstream conditions of a BZT flow far ahead of the airfoil. A map of Γ, Λ and Σ in the p/p_c vs. v/v_c coordinates is shown in figure 10. The whole area above the saturation curve may be divided into six possible zones by the $\Gamma = 0$, $\Lambda = 0$ and $\Sigma = 0$ curves. Table 1 shows the signs of Γ, Λ and Σ in these six zones. The circle in figure 10 indicates the intersection state where $\Gamma = \Lambda = 0$. At this point, the transonic flow pattern is described by a shock wave on the airfoil (as the results in §4.3 show). In the interest of expanding knowledge on the possible flow patterns of BZT gases, nine cases of transonic flows with various far-field pressures and densities in the neighbourhood of the $\Gamma = \Lambda = 0$ state are studied according to solutions (1). The upstream flow conditions for these cases are indicated by the squares in figure 10. In all of the cases, $R/c_v = 0.02$, the far-field Mach number $M_\infty = 0.97$ and the airfoil is NACA0012.

In zone I, where $\Gamma < 0$, $\Lambda > 0$ and $\Sigma > 0$, a compression shock wave appears near the mid-chord of the airfoil. A contour plot of the Mach number is shown in figure 11(*a*) and for this case the pressure drag coefficient $C_D = 0.03$.

In zone II, where $\Gamma < 0$, $\Lambda < 0$ and $\Sigma > 0$, an expansion shock wave is found near the airfoil's nose region along with a detached shock wave in front of it (see figure 11*b*). For perfect gases, it is well-known that only a supersonic flow can have a detached shock wave; however, in BZT gas flows, owing to the faster decrease in speed of sound than in velocity when $\Gamma < 0$, a supersonic speed zone appears just in front of the airfoil and creates a detached shock wave. Since a detached shock wave is usually larger and stronger than any shock wave on the airfoil, a relatively large computational domain is needed to compute this flow problem. For this flow case, the pressure drag coefficient is relatively large, $C_D = 0.13$.

In zone III, where $\Gamma < 0$, $\Lambda < 0$ and $\Sigma < 0$, several shock waves are found (see figure 11*c*). They include a detached shock wave ahead of the airfoil, an expansion

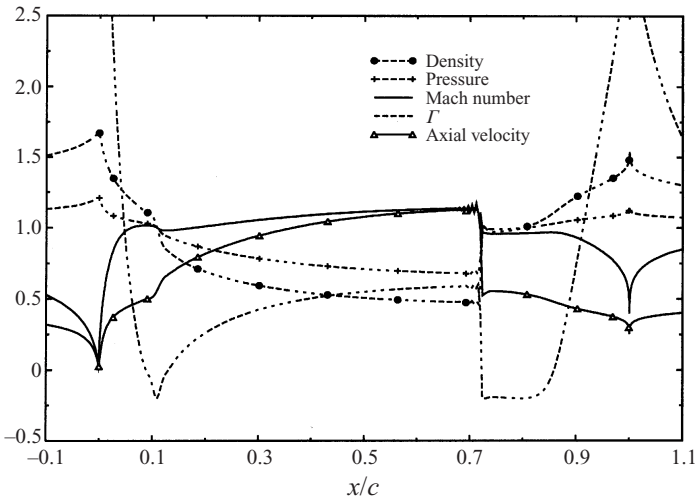

FIGURE 12. An expansion shock wave and a compression shock wave on a NACA0012 airfoil; $p_\infty/p_c = 1.045, v_\infty/v_c = 1.315$.

shock wave on the front section of the airfoil, a compression shock wave on the mid-section of the airfoil, a tail compression shock wave at the trailing edge, and an expansion wake shock wave behind the airfoil. For this flow case, the pressure drag coefficient is also relatively large, $C_D = 0.17$, due to the appearance of several shock waves.

In zones IV and V, where $\Gamma > 0$ and $\Sigma > 0$, a compression shock wave appears near the end of the trailing edge in each case. The Mach number contour plots are shown in figures 11(*d*) and 11(*e*). For these flow cases, the pressure drag coefficient is also relatively large, $C_D = 0.14$ for zone IV and $C_D = 0.16$ for zone V, due to the appearance of a large shock wave near the airfoil's trailing edge.

In zone VI, $\Gamma > 0$, $\Lambda < 0$ and $\Sigma < 0$. In the part of region VI near zone III, even though Γ is positive at the far field, it changes its sign locally in the airfoil region owing to the fact that $\Sigma < 0$. A detached shock wave, an expansion shock wave, and a compression shock wave are found (see figure 11*f*). For this flow case, the pressure drag coefficient is very large, $C_D = 0.22$, due to the appearance of several shock waves, specifically, of a strong expansion shock wave.

Far from the state of $\Gamma = \Lambda = 0$ in zone VI, when $p_\infty/p_c = 0.8$ and $v_\infty/v_c = 2.5$, the flow pattern is more like that of a perfect gas, with a strong tail shock wave. For this flow case (not shown here) the pressure drag coefficient is large, $C_D = 0.14$.

In summary, it can be seen that in the various near-sonic flow cases, the flow fields are characterized by the appearance of compression and, in some cases, expansion shock waves. Therefore, this usually results in large values of the pressure drag coefficient. It seems that zone (1) provides better conditions for the operation of the airfoils since the pressure drag is relatively low.

4.5. *Expansion shock wave case*

Out of the six possible zones described in figure 10 and table 1, we concentrate here on zone (I). The unique phenomenon of the expansion shock wave in the BZT gas flow is shown in figure 12. In this case, $M_\infty = 0.9999$, $\Gamma_\infty = -1.09$, $\Lambda_\infty = 0.72$, and $\Sigma_\infty = 24.07$ for which $p_\infty/p_c = 1.045$ and $v_\infty/v_c = 1.315$. The comparison of the solutions of the pressure coefficient according to the TSD, composite and Euler solvers

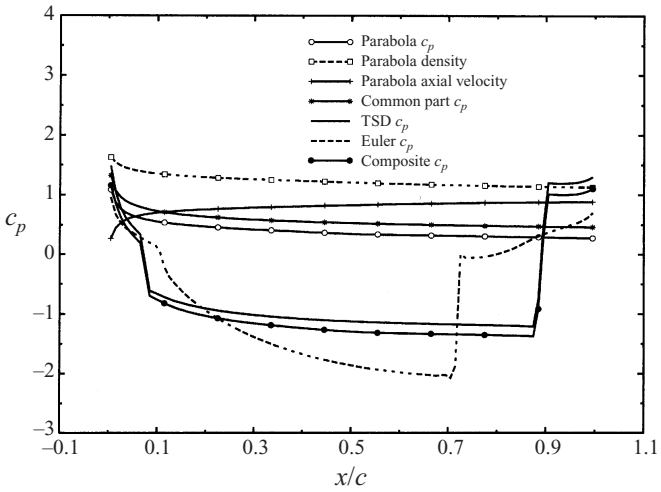

FIGURE 13. The comparison of pressure coefficient distribution on a NACA0012 airfoil according to composite and Euler solutions in the case with an expansion shock wave.

is shown in figure 13. It can be seen that the TSD solver captures the expansion shock wave near 10% of the airfoil's chord and the strength of the compression shock wave near the trailing edge. Owing to the entropy production behind the expansion shock wave, the composite solution deviates from the Euler solution after the expansion shock wave.

5. Conclusions and discussion

Numerical studies of two-dimensional, transonic flows of BZT gases around thin airfoils have been presented. These computations are guided by a recent asymptotic theory of Rusak & Wang (1997). A new TSD equation solver has been developed and provides solutions for the nonlinear BZT gas flow in the outer region around most of the airfoil. Numerical results of the composite solutions calculated from the asymptotic formula show agreement with the solutions of the Euler equations. This agreement demonstrates that the theoretical and numerical approaches support one another. It also provides clear insight into the special behaviour of the numerical solutions. The comparison between the solutions demonstrates that, in the leading order, TSD solutions of BZT gas flows represent the essence of the flow character computed from the Euler equations, including the appearance of expansion shock waves. Guided by the asymptotic formula, the computational results also demonstrate the similarity rules for transonic flow of BZT gases. There are some differences between the self-similar cases that may be related to the error in the asymptotic solution.

According to the assumptions made in § 2, where $\Gamma \sim 0$ and $\Lambda \sim 0$, it is found that the asymptotic solution for transonic flow of the BZT gases has a better agreement with the Euler solution in the region where K_Γ and K_Λ are of $O(1)$. Figure 14 shows the range of the region, $1.03 \leqslant p/p_c \leqslant 1.12$ and $1.3 \leqslant v/v_c \leqslant 1.5$, where the composite solutions are expected to have a better agreement with the solutions of the Euler equations. It is a limited range around the $\Gamma = \Lambda = 0$ state.

The discussion on the flow patterns around a NACA0012 airfoil at transonic speeds and at various upstream thermodynamic conditions shows that complicated and non-classical flow structures may appear. It also reveals that operating in the region around $\Gamma = \Lambda = 0$ results in lower pressure drag and higher critical Mach

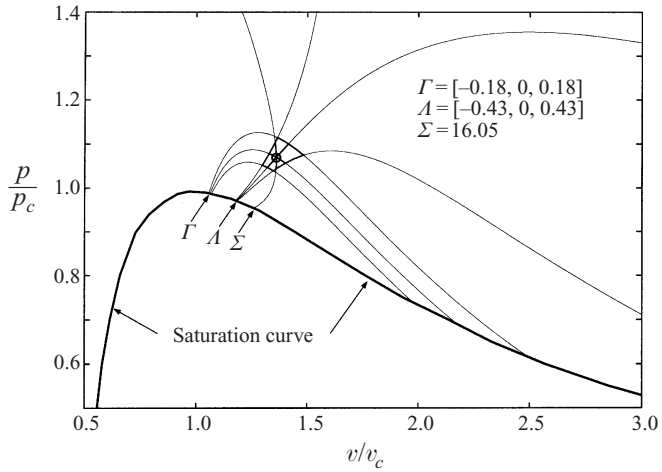

FIGURE 14. The region of Γ, Λ and Σ for a van der Waals gas with $R/c_v = 0.02$ where the composite solution is valid.

numbers. The results provide important guidelines for future experimental studies on this subject.

The present work is limited to an inviscid two-dimensional study. From the experience with perfect gas flows, it is expected that the addition of small viscosity will only add a nearly constant viscous drag to the pressure drag of the airfoils when the thickness parameter is above about 5%. Therefore, the present results may apply to high Reynolds number flows around such profiles. However, for the 2% thickness airfoils it is expected that the viscous drag is more dominant and the present results may not provide accurate information on the flow behaviour around such profiles.

Finally, for better results in approximating the BZT gas behaviour in transonic flow, an analytical study that includes the second- and third-order terms is suggested. This may help in improving the accuracy of computations using the asymptotic approach, specifically for airfoils with $\epsilon > 0.1$. Also, the asymptotic theory is limited to the region around $\Gamma = \Lambda = 0$. Developing extended theories for a wider range of thermodynamic conditions will help to increase our understanding of the complicated phenomena in compressible flow of dense gases. The flow pattern study shows that there are many more non-classical flow phenomena in compressible flow of BZT gases that are not quite understood and should be explored in the future using a combination of theoretical, numerical and experimental studies. Further understanding of those phenomena will provide essential knowledge for future utilization of such flows in mechanical and aeronautical applications.

The authors would like to thank Professor Mark S. Cramer for providing them with the computer code of Morren (1990) and for many insightful discussions on the topic. The authors also thank Dr Grey M. Tarkenton for helpful discussions. The first author (C.-W. Wang) wishes to thank the Chung-Cheng Institute of Technology (CCIT) in Taiwan for supporting his graduate studies.

Appendix

We derive here the thermodynamic fundamental derivative, Γ, the second derivative, Λ, and the third derivative, Σ, for a van der Waals gas. The general form of entropy

in terms of the pressure, temperature, and density is given by

$$\mathrm{d}s = c_v \frac{\mathrm{d}T}{T} - \left(\frac{\partial p}{\partial T}\right)_\rho \frac{\mathrm{d}\rho}{\rho^2}.$$

From the van der Waals equation of state,

$$p = \frac{\rho R T}{1 - b\rho} - \alpha\rho^2, \tag{A 1}$$

we have

$$\left(\frac{\partial p}{\partial T}\right)_\rho = \frac{\rho R}{1 - b\rho},$$

and so

$$\mathrm{d}s = c_v \frac{\mathrm{d}T}{T} - \left(\frac{R}{1 - b\rho}\right) \frac{\mathrm{d}\rho}{\rho}.$$

Integrating this equation with respect to a reference state where $\rho_r = \rho_\infty$ and $s_r = s_\infty$, we have

$$\frac{s - s_\infty}{c_v} = \ln\left(\frac{T}{T_\infty}\right) + \frac{R}{c_v} \ln\left[\left(\frac{1 - b\rho}{\rho}\right)\left(\frac{\rho_\infty}{1 - b\rho_\infty}\right)\right].$$

Here, from (A 1)

$$T_\infty = \frac{(1 - b\rho_\infty)(p_\infty + \alpha\rho_\infty^2)}{\rho_\infty R}. \tag{A 2}$$

The non-dimensional parameters are defined

$$\bar{\rho} = \frac{\rho}{\rho_\infty}, \quad \bar{p} = \frac{p}{p_\infty}, \quad \bar{\alpha} = \frac{\alpha\rho_\infty^2}{p_\infty}, \quad \bar{b} = b\rho_\infty; \tag{A 3}$$

then the entropy equation becomes

$$\bar{s} \equiv \exp\left(-\frac{s - s_\infty}{c_v}\right) = \left(\bar{\rho}\frac{1 - \bar{b}}{1 - \bar{b}\bar{\rho}}\right)^{1 + R/c_v} \left(\frac{1 + \bar{\alpha}}{\bar{p} + \bar{\alpha}\bar{\rho}^2}\right). \tag{A 4}$$

Thus, the non-dimensional pressure is

$$\bar{p} = \left(\frac{1 + \bar{\alpha}}{\bar{s}}\right)\left(\bar{\rho}\frac{1 - \bar{b}}{1 - \bar{b}\bar{\rho}}\right)^{1 + R/c_v} - \bar{\alpha}\bar{\rho}^2. \tag{A 5}$$

From (A 3) and (A 5), we can derive the speed of sound for the van der Waals equation of state in an isentropic flow as

$$a^2 = \left.\frac{\partial p}{\partial \rho}\right|_s = \frac{RT}{(1 - b\rho)^2}\left(1 + \frac{R}{c_v}\right) - 2\alpha\rho. \tag{A 6}$$

For the speed of sound at the far field, from (A 2), (A 3) and (A 6), we have

$$a_\infty^2 = \frac{p_\infty}{\rho_\infty}\left[\left(\frac{1 + \bar{\alpha}}{1 - \bar{b}}\right)\left(1 + \frac{R}{c_v}\right) - 2\bar{\alpha}\right] = \frac{p_\infty}{\rho_\infty} B, \tag{A 7}$$

where B is a constant associated with the gas characteristics and is shown in (A 7) inside the square brackets. From (A 3) and (A 5)–(A 7), the non-dimensional speed of sound is

$$\begin{aligned}\bar{a}^2 = \frac{a^2}{a_\infty^2} &= \frac{1}{B}\left[\left(\frac{\bar{p} + \bar{\alpha}\bar{\rho}^2}{\bar{\rho}(1 - \bar{b}\bar{\rho})}\right)\left(1 + \frac{R}{c_v}\right) - 2\bar{\alpha}\bar{\rho}\right] \\ &= \frac{1}{B}\left[(1 - \bar{b}\bar{\rho})^{-2 - R/c_v}\bar{\rho}^{R/c_v} N - 2\bar{\alpha}\bar{\rho}\right]\end{aligned} \tag{A 8}$$

where

$$N = \left(\frac{1+\bar{\alpha}}{\bar{s}}\right)(1-\bar{b})^{1+R/c_v}\left(1+\frac{R}{c_v}\right) = \text{constant}.$$

Since

$$\Gamma \equiv 1+\frac{\rho}{a}\left.\frac{\partial a}{\partial \rho}\right|_s = 1+\frac{\bar{\rho}}{\bar{a}}\left.\frac{\partial \bar{a}}{\partial \bar{\rho}}\right|_{\bar{s}},\ \Lambda = \rho\frac{\partial \Gamma}{\partial \rho} = \bar{\rho}\frac{\partial \Gamma}{\partial \bar{\rho}} \text{ and } \Sigma = \rho\frac{\partial \Lambda}{\partial \rho} = \bar{\rho}\frac{\partial \Lambda}{\partial \bar{\rho}},$$

we can find the derivatives of the speed of sound with density as follows:

$$\left.\frac{\partial \bar{a}}{\partial \bar{\rho}}\right|_{\bar{s}} = \frac{\bar{a}}{\bar{\rho}}(\Gamma-1), \tag{A 9}$$

$$\left.\frac{\partial\left(\bar{a}^2\right)}{\partial \bar{\rho}}\right|_{\bar{s}} = 2\frac{\bar{a}^2}{\bar{\rho}}(\Gamma-1), \tag{A 10}$$

$$\left.\frac{\partial^2\left(\bar{a}^2\right)}{\partial \bar{\rho}^2}\right|_{\bar{s}} = \frac{\bar{a}^2}{\bar{\rho}^2}(4\Gamma^2-10\Gamma+2\Lambda+6), \tag{A 11}$$

and

$$\left.\frac{\partial^3\left(\bar{a}^2\right)}{\partial \bar{\rho}^3}\right|_{\bar{s}} = \frac{\bar{a}^2}{\bar{\rho}^3}(8\Gamma^3-36\Gamma^2+52\Gamma+12\Gamma\Lambda-18\Lambda+2\Sigma-24). \tag{A 12}$$

From the definition and (A 8), the fundamental derivative of gasdynamics, Γ, is

$$\Gamma = \frac{1}{B\bar{a}^2}\left[N\bar{\rho}^{R/c_v}(1-\bar{b}\bar{\rho})^{-3-R/c_v}\left(1+\frac{R}{2c_v}\right)-3\bar{\alpha}\bar{\rho}\right]. \tag{A 13}$$

At the far field, where $\bar{\rho}=\bar{p}=\bar{s}=\bar{a}=1$ and $\Gamma_\infty = 0$, we have

$$\bar{b} = 1-\left[\left(\frac{1+\bar{\alpha}}{3\bar{\alpha}}\right)\left(1+\frac{R}{c_v}\right)\left(1+\frac{R}{2c_v}\right)\right]^{1/2}. \tag{A 14}$$

Also, from the formula for Γ, (A 8), and (A 10), the second derivative of gasdynamics is

$$\Lambda = -2\Gamma^2+3\Gamma+\frac{N}{B\bar{a}^2}\bar{\rho}^{R/c_v}(1-\bar{b}\bar{\rho})^{-4-R/c_v}\left(1+\frac{R}{2c_v}\right)\left(\frac{R}{c_v}-1+4\bar{b}\bar{\rho}\right). \tag{A 15}$$

For the far-field conditions of $\Gamma_\infty = \Lambda_\infty = 0$, we find

$$\bar{b} = \frac{1-R/c_v}{4}$$

and

$$\bar{\alpha} = \frac{16\left(1+R/c_v\right)\left(1+R/2c_v\right)}{11\left(1-R/c_v\right)\left(1+\frac{5}{11}R/c_v\right)}.$$

From (A 10)–(A 12), the third derivative of gasdynamics is

$$\Sigma = -4\Gamma^3+10\Gamma^2-6\Gamma-6\Gamma\Lambda+5\Lambda+\frac{N}{B\bar{a}^2}\bar{\rho}^{R/c_v}\left(1-\bar{b}\bar{\rho}\right)^{-5-R/c_v} \times\left(1+\frac{R}{2c_v}\right)\left[\left(\frac{R}{c_v}+4\bar{b}\bar{\rho}\right)^2-\frac{R}{c_v}-4\bar{b}^2\bar{\rho}^2\right]. \tag{A 16}$$

Also, the general form of internal energy (e) in terms of the pressure, temperature and density is given by

$$\mathrm{d}e = c_v \mathrm{d}T - \left(T \frac{\partial p}{\partial T}_{\rho} - p \right) \frac{\mathrm{d}\rho}{\rho^2}.$$

For the van der Waals gas model with a constant c_v, we find

$$e - e_\infty = c_v(T - T_\infty) - \alpha(\rho - \rho_\infty)$$

and from the enthalpy definition

$$h - h_\infty = c_v T_\infty \left(\frac{T}{T_\infty} - 1 \right) - 2\alpha(\rho - \rho_\infty) + \frac{RT_\infty}{1 - b\rho_\infty} \left(\frac{T}{T_\infty} \frac{1 - b\rho_\infty}{1 - b\rho} - 1 \right).$$

Using the van der Waals equation (A 1) and the formula for $\bar{p}$ derived above, we can compute

$$\left. \frac{T}{T_\infty} \right|_{s=s_\infty} = \left(\frac{\rho}{\rho_\infty} \frac{1 - b\rho_\infty}{1 - b\rho} \right)^{R/c_v}$$

from which the enthalpy as function of density in an isentropic flow $s = s_\infty$ can be computed. To be more specific,

$$\overline{T} = \frac{T}{T_\infty} = \frac{\bar{p} + \bar{\alpha}\bar{\rho}^2}{\bar{\rho}} \frac{1 - \bar{b}\bar{\rho}}{(1 + \bar{\alpha})(1 - \bar{b})}, \tag{A 17}$$

$$\frac{h - h_\infty}{a_\infty^2} = \frac{1}{B} \left\{ \frac{c_v}{R}(1 + \bar{\alpha})(1 - \bar{b})(\overline{T} - 1) - 2\bar{\alpha}(\bar{\rho} - 1) + (1 + \bar{\alpha}) \left(\frac{\overline{T}(1 - \bar{b})}{1 - \bar{b}\bar{\rho}} - 1 \right) \right\}. \tag{A 18}$$

REFERENCES

Abramowitz, M. & Stegun, I. A. 1965 *Handbook of Mathematical Functions*. Dover.

Bethe, H. A. 1942 The theory of shock waves for an arbitrary equation of state. *Office of Scientific Research and Development*, *Rep.* 545.

Cole, J. D. & Cook, L. P. 1986 *Transonic Aerodynamics*. North-Holland.

Cramer, M. S. 1989 Negative nonlinearity in selected fluorocarbons. *Phys. Fluids* A **1**, 1894–1897.

Cramer, M. S. 1991 On the Mach number variation in steady flows of dense hydrocarbons. *Trans. ASME: J. Fluids Engng* **113**, 675–680.

Cramer, M. S. & Fry, R. 1993 Nozzle flows of dense gases. *Phys. Fluids* A **5**, 1246–1259.

Cramer, M. S. & Tarkenton, G. M. 1992 Transonic flows of Bethe–Zel'dovich–Thompson fluids. *J. Fluid Mech.* **240**, 197–228.

Devotta, S. & Holland, F. A. 1985 Comparison of theoretical Rankine power cycle performance data for 24 working fluids. *Heat Recovery Systems* **5**, 503.

Duhem, P. 1909 Sur la propagation der ondes de choc au sien des fluids. *Z. Phys. Chem., Leipzig* **69**, 169–186.

Jameson, A. & Yoon, S. 1986 Multigrid solution of the Euler equations using implicit schemes. *AIAA J.* **24**, 1737–1743.

Kluwick, A. 1993 Transonic nozzle flow in dense gases. *J. Fluid Mech.* **247**, 661–688.

Kuethe, A. M. & Chow, C. Y. 1986 *Foundations of Aerodynamics*, 4th Edn. John Wiley & Sons.

Martin, J. J. & Hou, Y. C. 1955 Development of an equation of state for gases. *AIChE J.* **1**, 142–151.

Moran, M. J. & Shapiro, H. N. 1992 *Fundamentals of Engineering Thermodynamics*, 3rd Edn. John Wiley & Sons.

Morren, S. H. 1990 Transonic aerodynamics of dense gases. MSc thesis, Engineering Science and Mechanics Department, Virginia Polytechnic Institute and State University (also appeared as *NASA TM* 103732, 1991).

Murman, E. M. & Cole, J. D. 1971 Calculation of plane steady transonic flows. *AIAA J.* **9**, 114–121.

Redlich, O. & Kwong, J. N. S. 1949 On the thermodynamics of solutions V. An equation of state fugacities of gaseous solutions. *Chem. Rev.* **44**, 233.

Rusak, Z. 1993 Transonic flow around the leading edge of a thin airfoil with a parabolic nose. *J. Fluid Mech.* **248**, 1–26.

Rusak, Z. & Wang, C. W. 1997 Transonic flow of dense gases around an airfoil with a parabolic nose. *J. Fluid Mech.* **346**, 1–21.

Schnerr, G. H. & Leidner, P. 1993 Real gas effects on the normal shock behaviour near curved walls. *Phys. Fluids* **5**, 2996–3003.

Tarkenton, G. M. & Cramer, M. S. 1993 Transonic flows of dense gases. *ASME* 93-FE-9.

Thompson, P. A. 1971 A fundamental derivative in gasdynamics. *Phys. Fluids* **14**, 1843–1849.

Thompson, P. A. & Lambrakis, K. 1973 Negative shock waves. *J. Fluid Mech.* **60**, 187–208.

Thompson, P. A. 1984 *Compressible Fluid Dynamics.* Advanced Engineering Series.

Wang, C. W. 1998 Transonic flow of dense gases around an airfoil. PhD dissertation, Department of Mechanical Engineering, Aeronautical Engineering and Mechanics, Rensselaer Polytechnic Institute.

Zel'dovich, Y. B. 1946 On the possibility of rarefaction shock waves. *Zh. Eksp. Teor. Fiz.* **4**, 363–364.

Zel'dovich, Y. B. & Raizer, Y. P. 1966 *Physics of Shock Waves and High Temperature Hydrodynamic Phenomena.* Academic.